Title

Practical design considerations for secondary air injection in wood-burning cookstoves: An experimental study

Authors

Caubel, JJ
Rapp, VH
Chen, SS
et al.

Publication Date

2020

DOI

10.1016/j.deveng.2020.100049

Peer reviewed

Practical Design Considerations for Secondary Air Injection in Wood-Burning Cookstoves: An Experimental Study

Julien J. Caubel†‡, Vi H. Rapp‡, Sharon S. Chen‡, Ashok J. Gadgil‡¶*

† Department of Mechanical Engineering, University of California, Berkeley, Berkeley, California 94720, United States

‡ Environmental Technologies Area, Lawrence Berkeley National Laboratory, Berkeley, California 94720, United States

¶ Department of Civil and Environmental Engineering, University of California, Berkeley, Berkeley, California 94720, United States

**1 Cyclotron Road MS 90R2121, Berkeley, CA 94720*

Phone: 01-510-495-2035; E-mail: jcaubel@berkeley.edu

Abstract

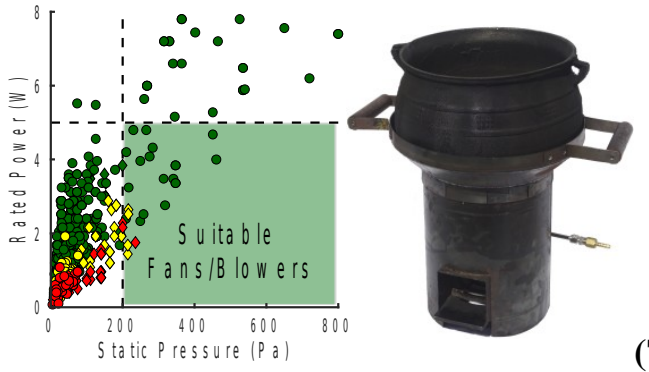

(TOC Art)

Billions of households worldwide cook using biomass fires and suffer from the toxic smoke emitted into their homes. Laboratory studies of wood-burning cookstoves demonstrate that secondary air injection can greatly reduce the emission of harmful air pollution, but these experimental advancements are not easily translated into practical cookstove designs that can be widely adopted. In this study, we use a modular cookstove platform to experimentally quantify the practical secondary air injection design requirements (e.g., flow rate, pressure, and temperature) to reduce mass emissions of particulate matter (PM), carbon monoxide (CO), and black carbon (BC) by at least 90% relative to a traditional cooking fire. Over the course of 111 experimental trials, we illuminate the physical mechanisms that drive emission reductions, and outline fundamental design principles to optimize cookstove performance. Using the experimental data, we demonstrate that low-cost (<$10) fans and blowers are available to drive the secondary flow, and can be independently powered using an inexpensive thermoelectric generator mounted nearby. Furthermore, size-resolved PM measurements show that secondary air injection inhibits particle growth, but the total number of particles generated remains

relatively unaffected. We discuss the potential impacts for human health and investigate methods to mitigate the PM formation mechanisms that persist.

Keywords: biomass cookstove; household energy; air pollution; design; combustion

1. Introduction

Over 2 billion people cook using solid biomass fuels, such as wood and dung.[1,2] Typically, households rely on traditional biomass cookstoves that are highly inefficient and polluting.[3,4] When these cookstoves are used in poorly ventilated homes, indoor concentrations of harmful pollutants, such as particulate matter (PM) and carbon monoxide (CO), can be up to 100 times higher than levels recommended by the World Health Organization (WHO).[5-7]

As a result, chronic exposure to indoor air pollution from solid biomass cookstoves is a leading environmental health risk, causing nearly 2 million premature deaths annually.[8,9]

Some biomass cookstoves are designed to reduce unwanted emissions by using a small fan or blower to inject secondary air into the combustion chamber.[10-14] When properly injected, the jets of secondary air increase the turbulent mixing and residence time of gas-phase fuel in the combustion zone, while providing oxygen directly to fuel-rich regions.[15-21] As a result, fuel oxidation is more complete, fewer harmful pollutants are emitted, and thermal efficiency is enhanced.[14,15] However, secondary air is typically much cooler than the exhaust gases and improper injection can result in lower combustion temperatures that limit fuel oxidation and heat transfer to the thermal load (e.g. a cooking pot).[19-23] For example, Jetter et al. evaluated the performance of several secondary air injection cookstoves and showed that half do not reduce PM or CO mass emissions relative to a three stone fire (TSF).[10]

Studies have shown that many secondary air injection design parameters, such as the flow rate and geometry, must be carefully considered and validated in order to significantly reduce unwanted emissions from biomass combustion appliances.[15,16,19-21,23-25] However, current studies do not usually consider the critical operational parameters needed to appropriately size the core

components of a practical, stand-alone cookstove. For example, no information is provided on the positive pressure required to drive the secondary air injection flow, although this information is required to select fans or blowers. Consequently, emission reductions achieved in the laboratory are not easily translated into cookstove designs that can be manufactured, distributed, and adopted on a large scale.

In this study, we use an experimental cookstove platform to investigate the practical secondary air injection design requirements for reducing the mass emission of air pollutants from unprocessed wood combustion by one order of magnitude. We conducted 111 experimental trials, systematically varying critical secondary air injection parameters (e.g. flow rate and location) to identify a design configuration that emits 90% less CO, PM, and (BC) than a TSF, and also improves thermal efficiency. We targeted mass emission reductions of at least 90% because indoor pollution concentrations from traditional biomass cooking easily exceed health guidelines by 10 times or more.[3,6,7,26] Throughout the experimental optimization, we recorded the secondary air injection flow rate, pressure and temperature to evaluate whether the performance improvements are practically achievable using inexpensive, off-the-shelf components that can be powered independently (e.g., small fans powered by a thermoelectric generator). Furthermore, we use size-resolved PM measurements to investigate the underlying physical mechanisms contributing to the reduction of total PM mass emissions and identify particle size ranges where further emission reductions are needed.

2. Materials and Methods

2.1 Modular Air Injection Cookstove Design: Version 2 (MOD2)

The MOD2 stove, presented in Figure 1, is a continuously fed, wood-burning cookstove that enables critical secondary air injection parameters to be modulated easily and repeatably. The MOD2 stove is the second design iteration of the modular (MOD) stove described by Caubel et al.,[20] and therefore shares the same general design architecture and accommodates the same cast-aluminum Darfuri cooking pot. The MOD2 stove has a cylindrical firebox, 15 cm (6 inch) in diameter, with an open fuel feed at the front. Primary air enters the firebox through the open fuel feed, and adjustable openings below the grate. Above the firebox, a conical chimney reduces to a 6.4-cm (2.5-inch) diameter throat located directly below the pot. An integrated air manifold surrounds the firebox and conical chimney assembly (Figure 1(c)). Secondary air is supplied to a port at the back of the manifold and is injected into the firebox through orifices drilled into the conical chimney. The conical chimney is removable, such that different air injection patterns can easily be drilled, installed, and tested (Figure 1(b)). The pot's height above the chimney throat is controlled using adjustable supports. The stove also incorporates a steel skirt that closely surrounds the pot to enhance the rate of heat transfer from the exhaust gases.

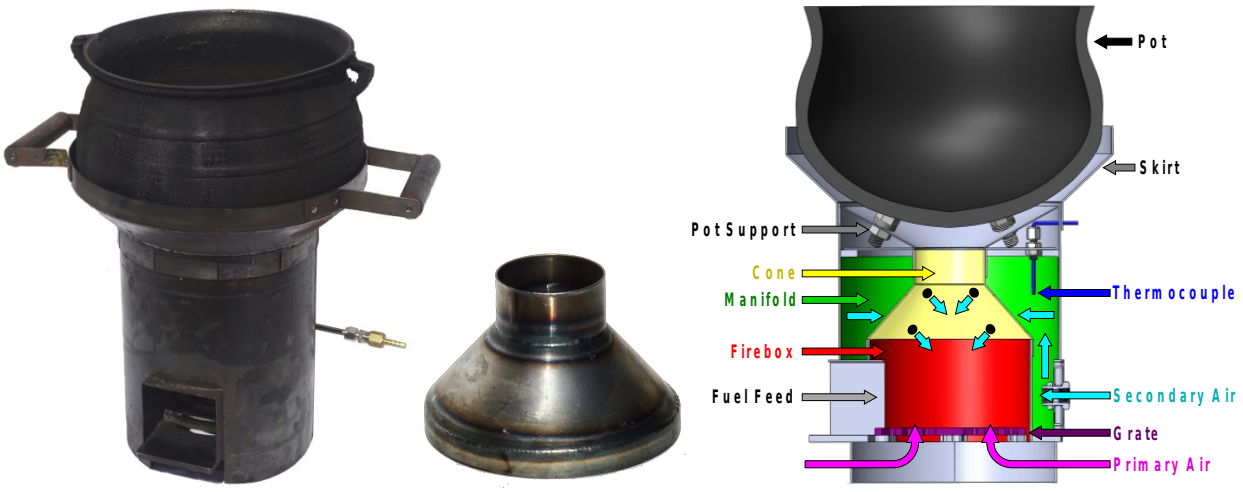

Figure 1. (a) The MOD2 stove with cast-aluminum Darfuri pot; (b) Removable conical chimney, into which secondary air injection patterns are drilled; (c) Cross-sectional view of the MOD2 stove showing the firebox, conical chimney, secondary air manifold, secondary air flow path, and other design features. Air injection holes are enlarged (out of scale) for clarity.

Previous research on the MOD stove (version 1) demonstrated that higher secondary air injection velocities improved stove performance, but excessive secondary flow quenched the combustion.[20] The velocity of the secondary air jets decreases rapidly after injection into the firebox. For the 1.59-mm (0.0625-inch) diameter secondary air injection orifices used throughout the MOD stove (version 1) study, the average jet velocity diminishes by 90% over a normal distance of just 4 cm,[27,28] or less than half of the distance required to reach the center of the MOD stove's firebox. To ensure that secondary air jets better reach the flames, the MOD2 stove's firebox and conical chimney diameters are approximately 15% smaller than in the MOD stove. By reducing the distance from the orifices to the combustion zone, the velocity of the air jets is higher when they reach the flames, thereby promoting turbulent mixing and oxygen injection at lower secondary flow rates that do not prohibitively cool the combustion. MOD2 stove dimensions were not reduced further, as a 15-cm firebox was deemed to be the smallest size that allows easy feeding and tending of the firewood. Additional details regarding the MOD2 stove design are provided in the SI.

2.2 Experimental Set-Up and Stove Testing Procedure

The MOD2 stove was developed at Lawrence Berkeley National Laboratory's (LBNL) cookstove testing facility. The experimental setup and testing procedure for the MOD2 stove are

the same as that described by Caubel et al. for the MOD stove (version 1),[20] and a brief overview is provided here. During testing, emissions from the MOD2 stove are completely captured using a steel hood, and exhausted outdoors using a steel ducting system and blowers. Air pollution instruments sample the duct flow and provide emission concentration measurements every second (1 Hz). A California Analytical Instruments 600 Series gas analyzer measures the volumetric concentrations (ppmv) of CO, carbon dioxide (CO_2), and oxygen (O_2). The total mass of $PM_{2.5}$ (PM with aerodynamic diameter $\leq$ 2.5 μm) emitted during the test phase is measured gravimetrically. A suite of real-time PM instruments sample emissions from the duct using a secondary diluter. A TSI 3091 Fast Mobility Particle Sizer (FMPS) and a TSI 3321 Aerodynamic Particle Sizer (APS) together provide size-resolved particle number concentration measurements from 5 to 2500 nm, while a Magee Scientific AE-22 Aethalometer provides black carbon (BC) mass concentration measurements. All instruments were calibrated according to manufacturer recommendations, as described by Caubel et al.[20]

The MOD2 stove was tested using the cold start, high power phase of the Water Boiling Test (WBT) 4.2.3 as pollutant emissions are usually highest during this phase of stove use.[20,29,30]

For each test, the MOD2 stove was initially at ambient temperature ("cold"), and a new fire was lit in a cold fuel bed (kindling). The stove was fueled with Douglas Fir wood cut into uniform 25 x 25 x 152-mm (1 x 1 x 6-inch) pieces and allowed to dry to 7-9% moisture content on a wet basis. Wood pieces were fed into the combustion chamber lengthwise, with one end slightly protruding from the open feed. The fuel feed rate was controlled to maintain a constant firepower setting of ~5 kW (monitored using real-time CO_2 concentration measurements from the exhaust duct) while bringing 5 L of cold water to a temperature of 99°C, the nominal local boiling point. Secondary air came from a compressed air cylinder. The standard volumetric flow

rate (SLPM) of secondary air was measured using a rotameter, and adjusted using a valve. The secondary air flow was initiated ~2 min after fuel ignition, once the kindling was observed to be fully lit, and was held constant throughout the remainder of the test. The secondary air temperature was monitored every second (1 Hz) using a thermocouple installed inside the stove manifold (Figure 1(c)). Manifold pressures were measured with a digital manometer through a dedicated tap.

2.3 Parametric Testing Procedure

Four MOD2 stove design parameters were systematically varied over a total of 111 tests: (1) secondary air injection pattern (2) secondary air injection flow rate (3) primary air intake, and (4) pot height. The first 52 tests were conducted to constrain the parametric space. Two promising air injection patterns were identified during these preliminary tests, shown in Figure A4 (a total of 7 patterns were tested). Pattern 1 consisted of two concentric rows, each with three orifices evenly spaced around the circumference of the conical chimney. The bottom row of orifices was located just above the firebox, while the top was directly below the throat. Pattern 2 was identical, except that the bottom row had six evenly spaced orifices, rather than three. All air injection orifices had a diameter of 1.59 mm (0.0625 inch). The primary air intake (the size of the inlet area under the grate) and pot height were also set during the preliminary tests, according to the experimental procedures and results provided in the SI.

For the remaining 59 parametric tests, the primary air intake was set to the fully open position and the pot height was held at 25 mm (except for the first 13 tests, when the pot was set 2 to 5 mm lower). Using these settings, both air injection patterns were tested at six secondary air flow rate settings ranging from 14 to 50 SLPM (0.5 to 1.75 SCFM), for a total of 12 parametric configurations. Four to eight replicate tests were conducted at each configuration (except for

Pattern 2 at 50 SLPM, with only 2 tests). When calculating configuration-average performance and emission metrics using this number of replicate tests, corresponding two-sided 90% confidence intervals were most often < 20% (± 10%) of the configuration-average values. This level of statistical confidence was deemed sufficient to enable meaningful comparisons. During testing, we discovered that the stove's air manifold leaked at the juncture between the removable conical chimney and the stove body (Figure A2). However, the leakage was consistent and replicable, and so the secondary flow actually injected into the firebox could be accurately calculated (see the procedure outlined in the SI). The calculations show that 27% to 39% of the total secondary flow was injected through the holes in the conical chimney, while the remainder leaked through the faulty manifold juncture, away from the firebox and combustion process. All results are presented in terms of the standard flow rate (SLPM) of air injected into the firebox, ranging from 5.5 to 14 SLPM, rather than the total flow into the manifold.

2.4 Data Analysis and Performance Metrics

All stove performance and emission metric calculations are presented in section S-1.4 of the SI. Emission factors are normalized by the average thermal power delivered to the pot, known as cooking power (kWd). All data are presented with 90% confidence intervals calculated using Student's t-distribution.[31,32] The MOD2 stove's performance and emissions are compared to those of the MOD stove (version 1) and a TSF, both tested using the same experimental procedure, fuel, cooking pot, and firepower setting (~5 kW).[20,21] All size-resolved particle emission measurements from the TSI 3321 APS are converted from aerodynamic to electrical mobility diameter, and combined with measurements from the TSI 3091 FMPS according to the methods outlined in Appendix A.

For both air injection patterns, the manifold pressure was measured at each secondary flow rate setting while the stove was cold, as described in Appendix A. Using real-time manifold temperature measurements and Equation 1 below, stove manifold pressures during each test were extrapolated from the corresponding pressure measurement recorded while the stove was cold.

$$\Delta P(t) = \Delta P_{STP}\left(\frac{\rho_{STP}}{\rho(t)}\right) = \frac{\Delta P_{STP}\,\rho_{STP}\left(T_{man}(t)+273\right)R_{air}}{P_{man}} \quad (1)$$

ΔP(t) (Pa) is the manifold gauge pressure at sample time 't', ΔP_{STP} (Pa) is the manifold gauge pressure measured at ambient conditions (show in Figure A6), ρ_{STP} is the density of air at standard conditions (1.225 kg/m^3), $T_{man}(t)$ (°C) is the air temperature in the manifold at sample time 't', R_{air} is the ideal gas constant for air (287 J/Kg K), and P_{man} is the absolute pressure in the manifold (roughly equal to the local ambient pressure, 97150 Pa). Average manifold pressures represent the mean of all one-second values calculated over the length of the cold start test.

3. Results and Discussion

3.1 Stove Performance and Emissions: Air Injection Pattern and Flow Rate

For both air injection patterns, Figure 2 shows that the MOD2 stove's thermal and emissions performance improve significantly as the secondary flow rate increases from 5.3 to 8.5 SLPM. Since firepower was held constant throughout testing, the average stoichiometric flow of air into the combustion reaction is ~70 SLPM for all design configurations (Figure B4), and the total flow of air through the stove may be 2-5 times higher than this stoichiometric value, as the wood combustion draws excess primary air.[24,33,34] Over this range of secondary flow rates, which account for 7.5 to 12% of the average stoichiometric air flow, CO, $PM_{2.5}$, and BC emissions drop by 55% to 75%, while combustion efficiency rises from 95% to 98%. These improvements

demonstrate that unprocessed wood combustion is highly sensitive to small changes in secondary flow (relative to the total combustion flow), as higher air jet velocities provide more turbulent mixing and oxygen in the combustion zone.[18] The improvement of combustion conditions also translates to gains in thermal efficiency, which increases from 29% to 32% over this range.

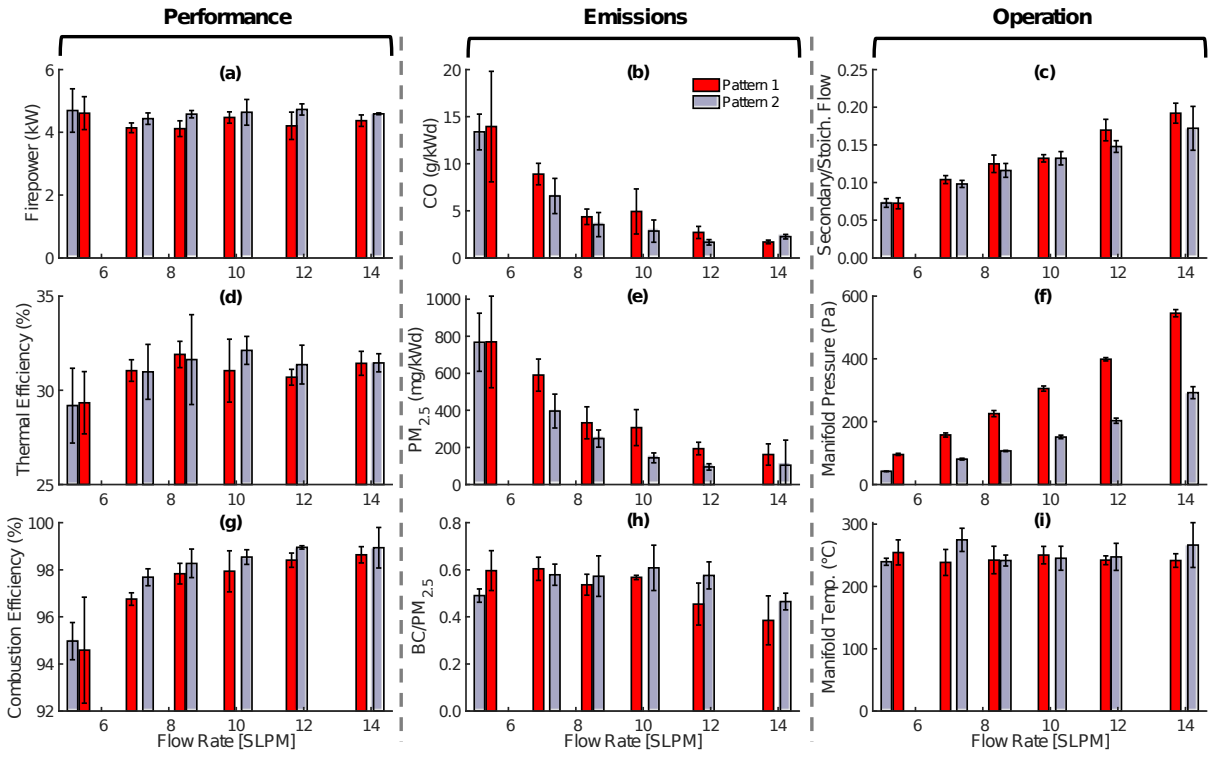

Figure 2. MOD2 stove performance, emissions, and operational metrics during high-power cold start testing, presented as function of secondary air injection pattern and flow rate: (a) Firepower (kW); (b) Carbon Monoxide (CO) emissions (g/kWd); (c) Ratio of the **s**econdary to stoichiometric flow rate of air; (d) Thermal efficiency (%); (e) Particulate matter ($PM_{2.5}$) emissions (mg/kWd); (f) Average manifold pressure (Pa); (g) Combustion efficiency (%); (h) Black Carbon (BC) to total $PM_{2.5}$ ratio; (i) Average manifold temperature (°C). Bars represent the mean of replicate test data collected for each stove configuration, while error bars represent the corresponding 90% confidence interval.

For secondary flow rates above 8.5 SLPM, thermal efficiency remains constant around 31%. At these settings, the secondary flow represents 12 to 18% of the average stoichiometric flow of air and is much colder than the exhaust gases. The average manifold temperature is roughly 250 °C for all configurations, while exhaust temperatures from biomass combustion typically exceed 850 °C.[16,24] Although the secondary air represents a small fraction of the total air flow into the stove, it may be sufficient at these settings (> 8.5 SLPM) to cool the exhaust gases appreciably, thereby limiting the rate of heat transfer to the pot. Other biomass cookstove studies show that exhaust temperatures drop with increased secondary flow.[16,22,35]

Some of the fire's thermal power output is also used to heat the secondary air in the manifold. Since average secondary air temperatures remain approximately constant for all configurations, more heat from the fire is necessarily transferred to the manifold as secondary flow increases. However, Figure B4 shows that less than 0.1 kW is lost to heating the secondary air at all flow rates, which is small compared to the average thermal power delivered to the pot (~1.4 kW). Therefore, secondary flow does not need to be constrained to maintain high air injection temperatures or prevent the diversion of output heat from the pot to the secondary air manifold, though some restraint is required to prevent excessive cooling of the exhaust gases.

Although thermal performance gains diminish with secondary flow rates above 8.5 SLPM, CO, $PM_{2.5}$, and BC emissions generally decrease steadily throughout the parametric range (Figure 2 and Figure B4), thereby suggesting that combustion temperatures remain sufficiently elevated to oxidize harmful pollutants, and higher air injection velocities continue to enhance mixing of the air and gas-phase fuel. Correspondingly, combustion efficiency increases from 98 to 99% as secondary flow rate increases above 8.5 SLPM, representing a further ~50% reduction in the fraction of carbon emitted as a product of incomplete combustion (CO).

244 However, average emissions of CO and $PM_{2.5}$ from Pattern 2 increase slightly at a flow rate of 14
245 SLPM. While only two tests were conducted in this configuration, the results suggest that
246 secondary flow rates above 12 SLPM through Pattern 2 may quench the flames, and reduce
247 combustion zone temperatures below the 850 °C required to oxidize CO and many of the volatile
248 organic species that form PM.[16,18,22] However, BC emissions continue to decrease in this stove
249 configuration, as the oxidation temperature of BC is much lower (~350 °C) than that of CO and
250 other pollutants,[36,37] and higher air injection velocities inhibit the formation of fuel-rich flame
251 zones where BC is formed.[38,39]

252 Emission reductions are not solely dependent on higher secondary air injection velocities
253 to enhance the combustion process. At each flow rate setting, the average injection velocity is
254 roughly 1.5 times greater through Pattern 1 than Pattern 2 (Figure B4), and yet Figure 2 shows
255 that Pattern 2 generally outperforms Pattern 1. This trend suggests that the addition of air jets
256 near the fuel bed promotes more effective turbulent mixing in the combustion zone, despite the
257 drop in injection velocity. In this way, wood combustion is also highly sensitive to the number of
258 secondary air injection orifices and their location relative to the fuel bed, and this sensitivity can
259 be exploited to enhance stove performance. For example, Figure 2 shows that the manifold
260 pressure at each flow rate setting is 1.9 to 2.3 times lower for Pattern 2 than for Pattern 1
261 (theoretically, the manifold pressure should be 2.25 times lower, as the air injection area 1.5
262 times greater). As a result, greater performance improvements are possible using lower
263 secondary flow rates and pressures that can be more easily provided by the miniature fans and
264 blowers typically found in improved cookstoves.

265 Figure 2 shows that a secondary flow rate of 12 SLPM through Pattern 2 minimizes the
266 MOD2 stove's CO and $PM_{2.5}$ emissions, while maximizing combustion efficiency. Although

thermal efficiency and BC emissions improve slightly (≤ 10% relative change) at other flow rate settings, this configuration likely provides an optimal balance between reducing harmful emissions and improving thermal performance. In this configuration, the MOD2 stove emits 90% less CO, $PM_{2.5}$, and BC than a TSF (on average), and thermal efficiency increases from 23±1% to 31±1% (Table S1).

While the MOD2 stove can be optimized to reduce biomass smoke emissions by roughly one order of magnitude (relative to a TSF), the ratio of BC to total $PM_{2.5}$ emissions ranges from 0.4 to 0.6 throughout the parametric range, which is higher than that typically reported for biomass cookstoves, both traditional and improved. [25,26,40,41] Initially, we suspected that these unusually elevated BC emission measurements might be the result of instrumentation error, although the Aethalometer was calibrated by the manufacturer prior to both experimental testing phases. Using calibration factors from the manufacturer and fundamental equations, we correctly replicated the instrument's BC concentration outputs from the underlying optical absorption and sample flow rate measurements. During this validation process, we did not uncover any indication that the instrument was operating incorrectly. Taken at face value, the high proportion of BC detected in the MOD2 stove emissions indicates that incomplete oxidation conditions persist.[17,25,42] However, BC is readily oxidized, and can be mitigated through improvements in the combustion process.[43] Therefore, it is important to identify the physical mechanisms responsible for these BC emissions such that they can be actively targeted in future designs.

The BioLite™ HomeStove™ is a wood-burning cookstove similar to the MOD2 stove that emits ~80% less $PM_{2.5}$ than the TSF presented here, and also has elevated $BC/PM_{2.5}$ ratios (>0.7).[11] These results suggest that rocket-style cookstoves with secondary air injection may oxidize most PM-forming species, but BC generation somehow persists. A likely explanation for

these persistent BC emissions is that the water-filled cooking pot is quenching flames protruding from the chimney throat.[44] When the MOD2 stove was operated without a pot skirt during preliminary tests, Figures B1 and B4 show that $PM_{2.5}$ emissions were comparable, but BC emissions were 2 to 3 times lower. Therefore, the $BC/PM_{2.5}$ ratio was significantly reduced (<0.25), though thermal efficiency also suffered without the pot skirt (< 29%). The pot skirt restricts the exhaust flow to enhance heat transfer, but the resultantly higher exhaust velocities entrain more flames through the chimney throat, where fuel-rich zones quench against the pot and emit BC. These results motivate further investigations that focus on preventing flame contact with the pot to reduce BC emissions while maintaining high thermal efficiency.

Compared to the MOD stove (version 1), the MOD2 stove achieves similar emission reductions at half the secondary air injection flow rate. Furthermore, when the secondary flow rate was set 25% higher than the optimal setting, $PM_{2.5}$ and CO emissions from the MOD stove more than doubled.[20] MOD2 stove emissions, on the other hand, increase only slightly (<40%) when the flow rate rises by ~17%, from 12 SLPM to 14 SLPM. Together, these trends illustrate that the MOD2 stove's smaller firebox and chimney dimensions allow the secondary air jets to be more effective at lower flow rates, penetrating further into the firebox to enable significant emission reductions while preventing excessive cooling or quenching of the combustion. Additionally, the lower secondary flow rates likely contribute to the MOD2 stove's higher thermal efficiency, as cooling of the exhaust flow diminishes.

Together, the experimental results demonstrate that the secondary air injection pattern and flow rate must be optimized to maximize the effective jet velocity but prevent flame quenching. Design compromises are also sometimes required to enhance both the stove's thermal and emissions performance. In this case, adding a pot skirt to the MOD2 stove enhanced thermal

efficiency but also increased the BC/$PM_{2.5}$ ratio. Since the MOD2 stove still achieves significant (90±10%) BC mass emission reductions relative to a TSF, the elevated BC/$PM_{2.5}$ ratio may be justified by the increase in thermal efficiency afforded. Having identified the optimal MOD2 stove design configuration and established the underlying physical mechanisms responsible for the performance improvements, it is important to determine whether these experimental results can be translated into a practical cookstove design that households can afford and adopt.

3.2 Secondary Air Injection Design Requirements: Flow, Pressure and Power

The MOD2 stove receives pressurized air from a cylinder, such that the secondary flow can be adjusted accurately and consistently over the course of many experimental trials, but this approach is clearly not practical or economical for typical household applications. Instead, many commercial biomass cookstoves rely on a small axial fan or centrifugal blower to drive the secondary flow, often drawing electrical power from a thermoelectric generator (TEG).[11,14] TEGs convert heat from the biomass combustion directly to electricity, thereby providing an independent, reliable, and convenient source of power at little cost (often < $10/W of power generated).[45-48] TEG modules mounted to biomass cookstoves have been shown to generate as much as 10 W of electrical power, although an output of 1 to 5 W is more typical.[45,47-49] There are also some biomass cookstoves powered by solar panels or simple wall chargers, but these alternatives are often less desirable, as they depend on operational factors external to the cookstove (such as sufficient insolation).

Figure 2 shows that MOD2 performance is optimal when injecting a secondary flow rate of 12 SLPM through Pattern 2. In this configuration, an average manifold pressure of ~200 Pa is required. As the stove heats up during normal use, higher manifold pressure is required to

maintain a constant mass flow of secondary air through the injection pattern. Air is injected into the MOD stove at room temperature (~25 to 30 °C) throughout, but reaches manifold temperatures of 300 to 400 °C during the cold start test (Figure 5). The density of air at these elevated temperatures is around half that of the air initially flowing into the manifold, and so the volumetric flow rate passing through the injection pattern effectively doubles, as does the manifold pressure required. Consequently, when sizing a fan or blower to drive secondary air injection in a biomass cookstove, it is important to consider the manifold pressure required at typical operating conditions, rather than when the stove is cold (at ambient temperature). In this study, we defined the operating temperature as the average secondary air temperature in the manifold during the cold start, and therefore we also present the average manifold pressure.

Figure 3 provides the maximum (static) pressure, maximum (free) flow rate, and rated electrical power consumption of 1,135 miniature fans and blowers stocked by Digi-Key Electronics®, a major electronic parts supplier.[50] This dataset is provided in Appendix B5. All available models costing < $10 (when ordering 1000 units) are presented, as the minimization of manufacturing costs is crucial to the development of affordable cookstoves. To reflect the MOD2 stove's operational requirements, reference lines are provided at a static pressure of 200 Pa and rated electrical power of 5 W (the maximum power typically output by a stove-mounted TEG module). The devices must operate near static conditions, or at a flow rate below ~10% of the maximum value specified by the manufacturer (measured with no flow resistance), to generate the maximum pressures presented in Figure 3. The MOD2 stove requires 12 SLPM in the optimal configuration, so the free flow rate should be at least ~100 LPM for the fan or blower to operate near static conditions. This target is based on a rough approximation of actual performance, so fans and blowers with a free flow rating ranging from 100 to 200 LPM (at

standard conditions) are represented using yellow markers (Figure 3) to indicate that some may not satisfy the 12 SLPM requirement under operational conditions. Green markers represent devices that are nearly certain to meet or exceed the stove's secondary flow rate requirement, while red markers indicate devices unlikely to meet the requirements. Since secondary air is drawn into the stove from the environment near standard conditions, the rated volumetric flow rate (LPM) is analogous to the stove's mass flow rate (SLPM) requirements, identified experimentally. It should also be noted that the rated power consumption is often measured at free flow conditions, and though this may not be exactly representative of power consumption at the requisite operating conditions (which will likely be larger as flow resistance is applied), it provides a valid estimate.

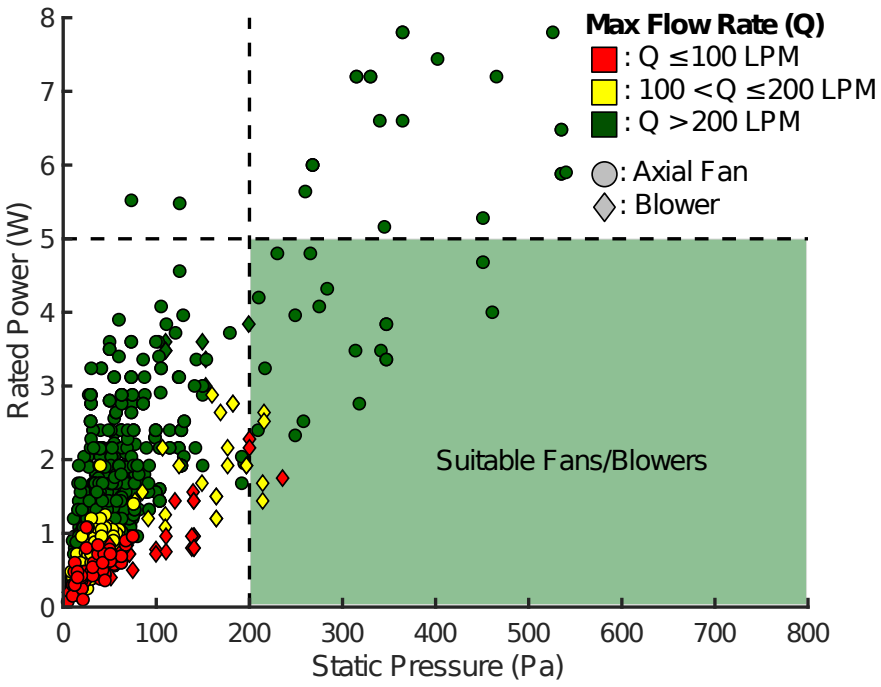

Figure 3. Static pressure, free flow rate, and rated electrical power consumption of 1,135 miniature axial fans and centrifugal blowers that are stocked by Digi-Key Electronics ® and cost < $10 per unit (when ordering 1000 units).[50] Fans and blowers that meet the MOD2 stove's

operational requirements (in the optimal design configuration) are indicated. Marker colors represent the devices' ability to operate near static flow conditions while providing the stove's required flow rate (12 SLPM).

Only 23 (~2%) of the 1,135 fans and blowers presented in Figure 3 meet the MOD2 stove's static pressure (>200 Pa), free flow (>100 SLPM), and electrical power (<5 W) requirements. Miniature fans and blowers are typically designed for cooling electronics, and therefore provide high air flow rates at low pressures – over 70% of the devices shown in Figure 3 generate maximum flow rates > 100 LPM using < 5 W of power, but at static pressures < 100 Pa. However, the MOD2 stove requires relatively low flow rates of air, driven through small orifices that generate high velocity air jets in the combustion chamber, but require high input pressures.

The small proportion of suitable fans and blowers illustrates the importance of carefully characterizing the cookstove's operational requirements. Using only knowledge of the air injection flow rate, as is usually provided in existing experimental studies, it is straightforward to select a fan or blower that meets the flow requirement, but provides insufficient positive pressure. Similarly, without manifold temperature measurements, it would be difficult to discern that the cookstove's volumetric flow rate and manifold pressure requirements double during normal operation. This analysis suggests that poorly performing cookstoves with secondary air injection may suffer from the implementation of inadequate fans and blowers, as operational guidelines are lacking.

Of the 23 viable devices identified, Figure 3 shows that suitable blowers generally require less power than axial fans, as they are better suited to high pressure, low flow applications. Overall, Figure 3 illustrates that low-cost fans and blowers are currently available to achieve effective and practical secondary air injection in wood-burning cookstoves, but they must be carefully chosen and evaluated, as the vast majority are not intended to meet the flow, pressure, and electrical power consumption conditions required.

3.3 Room for Improvement: Start Up and Ultrafine Particle Emissions

Health guidelines from the WHO, United States Environmental Protection Agency (US EPA), and other organizations generally recommend maximum $PM_{2.5}$ pollution levels in terms of mass concentration (e.g., $\mu g/m^3$). By this measure, the MOD2 stove should alleviate health impacts from biomass combustion, as it reduces $PM_{2.5}$ mass emissions by an order of magnitude relative to a traditional TSF. However, Figure 4 shows that the vast majority (>80%) of $PM_{2.5}$ emissions from the MOD2 stove consist of ultrafine particles (UFP) with a diameter < 100 nm, which may be particularly harmful to human respiratory health, as their small size enables deeper penetration into the lungs.[51-54] Consequently, it is important not only to reduce the mass of PM generated, but also the number of UFPs emitted and potentially inhaled.

Secondary air injection does not significantly reduce the total number of particles generated by biomass combustion, but instead shifts the PM size distribution towards smaller, less massive particles.[20,21,55,56] As the secondary flow rate increases from 7.2 to 12 SLPM, Figure 4 shows that the total number of particles emitted from 5 to 2500 nm remains relatively steady, ranging from 5.5×10^{14} to 6.9×10^{14} particles/kWd. Total $PM_{2.5}$ volume, on the other hand,

decreases over the range of secondary flow rates presented, as particle size diminishes. Given that $PM_{2.5}$ density remains nearly constant (Figure B4), the particle volume measurements are directly proportional to particle mass, and therefore closely mirror the $PM_{2.5}$ mass emission measurements shown in Figure 2.

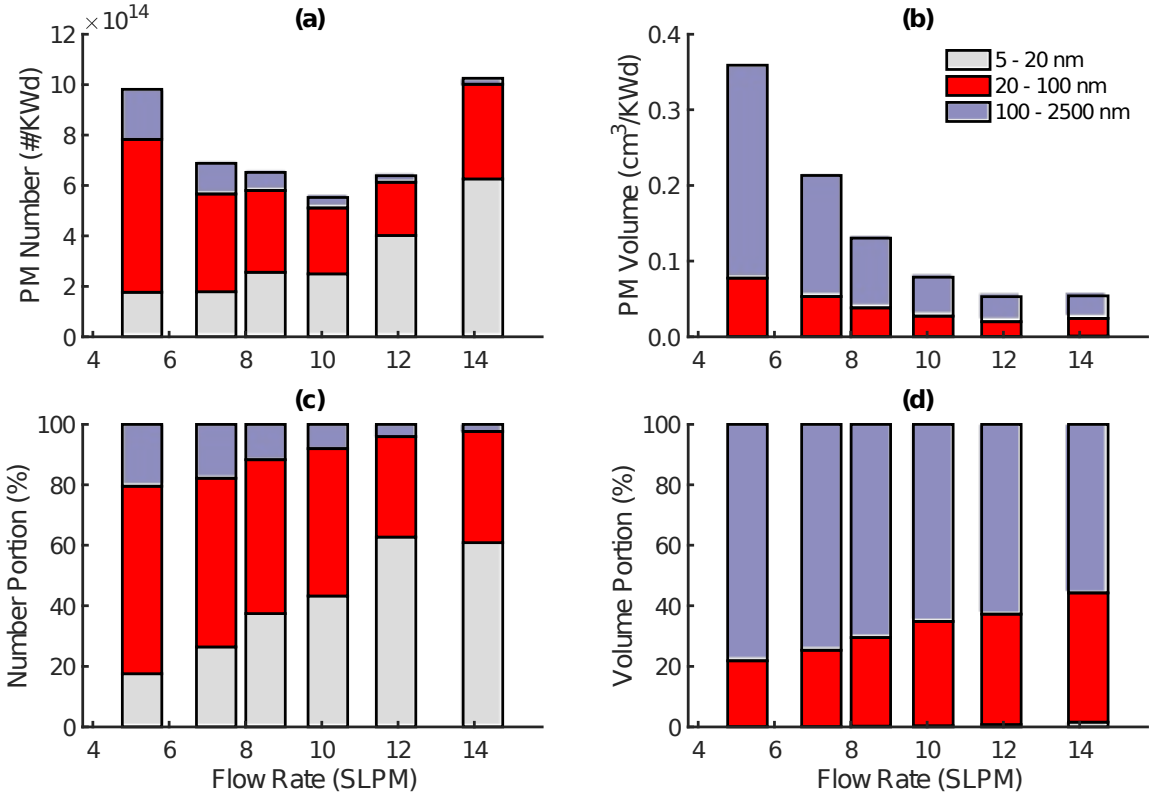

Figure 4. (a) Total $PM_{2.5}$ number and (b) volume emissions from the MOD2 stove over the cold start (normalized by cooking power), as a function of particle diameter and secondary flow rate through air injection Pattern 2. (c) Portion of the total number, and (d) volume of particles emitted in each particle diameter range: 5 to 20 nm, 20 to 100 nm, and 100 to 2500 nm. Each bar represents the mean of replicate test data collected for each stove configuration. Confidence intervals are omitted here for clarity, and instead provided in Figure B5.

Figure 4 shows that secondary air injection inhibits particle growth, but does not significantly reduce particle formation. Particles form either through nucleation, as volatile organic and inorganic compounds emitted during wood pyrolysis cool in the exhaust, or through soot (BC) generation in the flame.[15,39,43,57] Typically, these primary particles grow through agglomeration and condensation of volatile compounds. Figure 2 shows that CO and $PM_{2.5}$ mass reductions closely mirror one another as secondary flow rate increases, likely because CO and many-PM forming volatile organic compounds (e.g. PAH) oxidize under similar conditions.[41,42,58] The portion of PM in the nucleation mode (5 to 20 nm) increases from 20 to 60% as secondary air flow through Pattern 2 increases, likely because particles no longer grow by condensation as volatile organic gas emissions diminish. While number emissions of these small particles increase markedly, they account for less than 2% of the total PM volume, and therefore have little effect on the total mass emitted. Figure B9 provides the size distribution of particle number emissions, and shows a distinct peak at a particle diameter of ~12 nm that increases with secondary flow rate.

In the absence of volatile organic gases in the exhaust, inorganic and BC particles generally grow to sizes <100 nm through agglomeration.[38,42,44,59] Figure 4 shows that the fraction of total particle number emissions in the UFP range (5 to 100 nm) grows from 80 to 97% as secondary flow increases, and accounts for 20 to 40% of the PM volume generated. As the size distribution shifts towards smaller particles, the fraction of particles in the accumulation mode (100 to 2500 nm) correspondingly decreases from 20 to 3% over the parametric range presented, but still accounts for most (60 to 80%) of the emitted volume. Particles in the accumulation mode form as some growth pathways persist, such the condensation of gases in cool regions of the exhaust flow or agglomeration of particles under turbulent mixing conditions. Throughout the

parametric range, nearly all (>> 99.9%) particles emitted are smaller than 1000 nm (6). Larger particles (>1000 nm) account for 0.2 to 0.7% of the total particle volume, and likely consist of fly ash generated in the fuel bed and entrained in the exhaust flow.[39]

Total particle number emissions are lowest for a secondary flow rate of 10 SLPM (Figure 4), suggesting that this configuration may provide the optimal balance of turbulent mixing and high combustion temperatures to inhibit particle formation. However, total $PM_{2.5}$ volume generation continues to decrease at higher flow rates, as particle size diminishes. Furthermore, $PM_{2.5}$ number emissions increases sharply from 12 to 14 SLPM, again indicating that excessive secondary flow in this configuration quenches the combustion zone,[17] thereby promoting more PM nucleation. However, total $PM_{2.5}$ volume changes little, as PM emissions in the accumulation mode remain relatively constant. Together, these trends demonstrate that $PM_{2.5}$ mass emission reductions can be achieved while simultaneously generating more UFPs.

When the secondary air flow rate is sufficient, the particle size distribution increasingly shifts towards smaller, less massive particles as the stove, fuel, and exhaust gases warm up during the cold start test.[60] The injection of hotter secondary air at higher velocities also likely contributes to the shift towards smaller particle emissions, as injection velocity increases proportionally with manifold temperature (Equation A5). When the secondary flow rate setting through Pattern 2 increases, Figure 5 shows that particle volume generation is increasingly attenuated over the first 18 minutes of the cold start test, although the number of emitted particles accumulates steadily for all configurations. The $PM_{2.5}$ number and volume accumulation rates reflect the secondary flow dependence illustrated in Figure 4. Manifold temperatures rise more rapidly at higher flow rate settings (Figure 5(c)), thereby hastening the inhibition of particle growth. For flow rates $\geq$ 10 SLPM, the count median diameter (CMD) of particle emissions

decreases from around 60 nm to 20 nm over the first 18 minutes of the cold start (Figure B10), and so most of the particle volume is emitted during start up. At the optimal secondary flow rate setting of 12 SLPM, half of total volume emissions are emitted within the first ~7 minutes following ignition, representing only ~30% of the total test length (in this configuration, the average time to boil is 24±2 min). Consequently, if further PM mass reductions are sought, methods should be developed to enhance combustion conditions during start up.

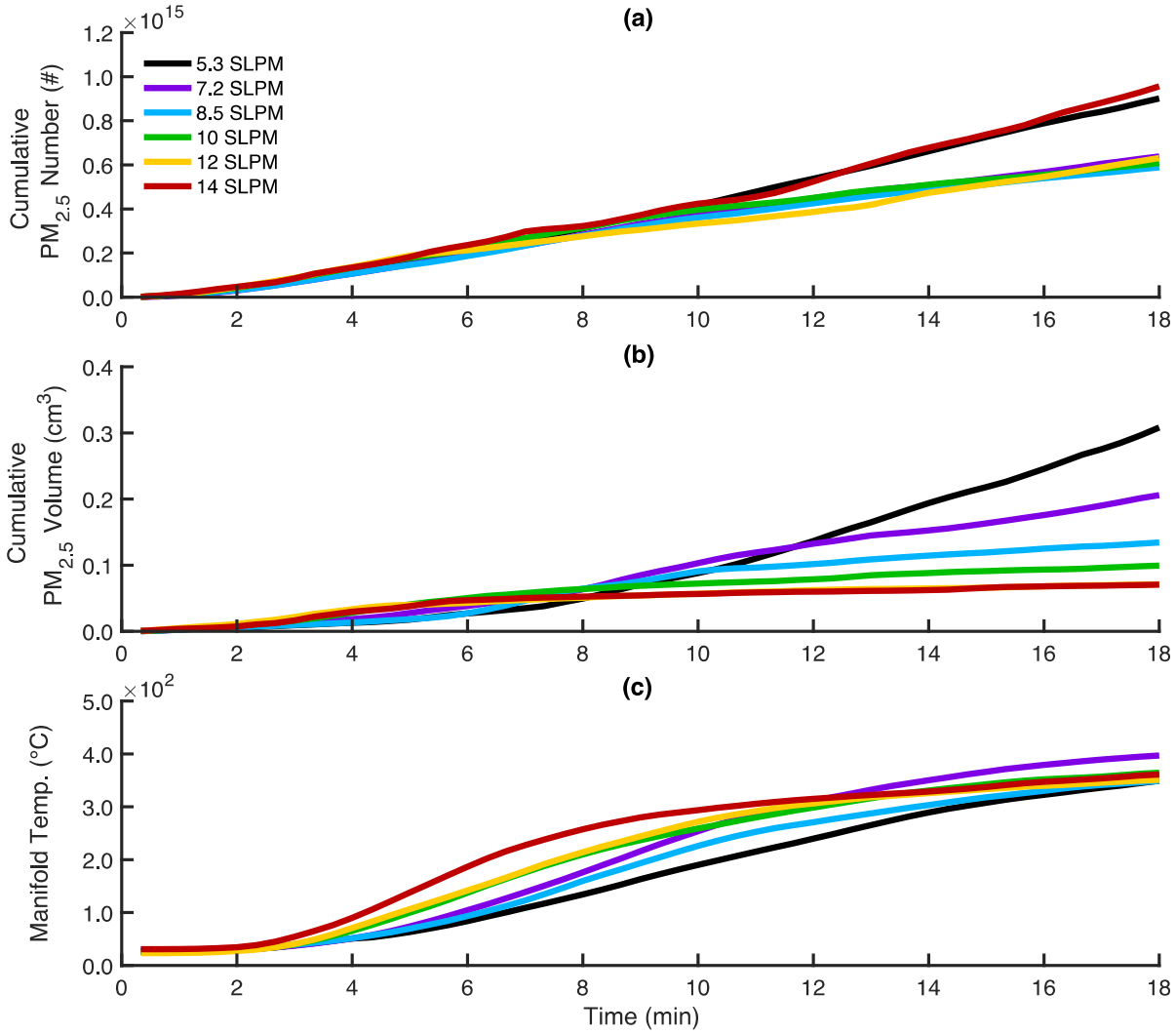

Figure 5. (a) Accumulation of $PM_{2.5}$ number and (b) volume emissions from the MOD2 stove over the first 18 minutes of the cold start test. (c) Temperature of secondary air in the MOD2 stove manifold over the same period. Each line represents the mean of replicate test measurements collected at each of the six secondary flow settings (using air injection Pattern 2). Confidence intervals are omitted here for clarity, and instead provided in Figures B7 and B8 for all secondary flow rate settings. All data presented is block-averaged on a 20-sec time base.

Although volume emissions are attenuated over time, the number of particles continues to accumulate steadily for all configurations, and the CMD is less < 80 nm throughout (Figure B10), well within the ultrafine range that is of particular concern for human health. As a result, it is important that future research efforts investigate methods for inhibiting particle formation entirely, rather than simply limiting particle growth. For example, methods of restricting the fuel bed temperature could be devised to limit the volatilization of inorganic compounds that nucleate into incombustible particles.[15]

4. Conclusion

While further improvements are needed to reduce UFP emissions, the MOD2 stove generally illustrates that secondary air injection is a practical and effective method for reducing mass emissions of $PM_{2.5}$, CO, and BC from wood combustion. Crucially, we show that emission reductions are achievable using inexpensive hardware that is currently on the market, and can be driven independently using a TEG or other low-cost power source. Stove performance is highly sensitive to secondary air injection design parameters, and so it is important that new designs be validated and optimized experimentally. The experimental results presented here illustrate

important design principles that will help to inform the development of clean, efficient, and practical cookstoves that better mitigate harmful air pollution exposure in the billions of households that depend on solid biomass for their daily cooking needs.

ACKNOWLEDGMENT

This work was performed at the Lawrence Berkeley National Laboratory, operated by the University of California, under DOE Contract DE-AC02-05CH11231. We gratefully acknowledge support for this work from DOE's Biomass Energy Technologies Office. Author Julien J. Caubel is grateful for support from the National Science Foundation's Graduate Research Fellowship Program.

The authors would like to recognize the central contribution of Allen Boltz, Marion Laglaive, Guillaume Charbonnel, Varun Khurana, Maelle Seigle and Anouar Mabrouk, who spent countless hours in the laboratory testing the cookstove and collecting the experimental data upon which this research is founded. We would also like to acknowledge the engineering staff at UC Berkeley and Lawrence Berkeley National Laboratory who fabricated the cookstove hardware: Alex Jordan, Jacob Gallego, Jeffrey Olson, Tim Williams, and Rick Kraft. Finally, we thank Dr. Daniel Wilson for his guidance in post-processing the particle emissions data and Gary Hubbard for developing the software tools to simplify data collection from all of our instruments.

DECLARATIONS OF INTEREST

None.

ABBREVIATIONS

APS, Aerodynamic Particle Sizer; BC, Black Carbon; CAI, California Analytical Instruments; CO_2, Carbon Dioxide; CO, Carbon Monoxide; FMPS, Fast Mobility Particle Sizer; kWd, kilowatt of thermal power delivered to the cooking pot; LBNL, Lawrence Berkeley National Laboratory; MOD, Modular Air Injection Stove: Version 1; MOD2, Modular Air Injection Stove: Version 2; PAH, Polycyclic Aromatic Hydrocarbon; PM, Particulate Matter; $PM_{2.5}$, Particulate Matter with an aerodynamic diameter $\leq$ 2.5 μm; ppmv, parts per million by volume; TEG, Thermoelectric Generator; TSF, Three Stone Fire; UFP, Ultrafine Particle; US EPA, United States Environmental Protection Agency; WBT, Water Boiling Test; WHO, World Health Organization.

REFERENCES:

(1) Bonjour, S.; Adair-Rohani, H.; Wolf, J.; Bruce, N. G.; Mehta, S.; Prüss-Ustün, A.; Lahiff, M.; Rehfuess, E. A.; Mishra, V.; Smith, K. R. Solid Fuel Use for Household Cooking: Country and Regional Estimates for 1980–2010. *Environ. Health Perspect.* **2013**, *121* (7), 784–790.

(2) Legros, G.; Havet, I.; Bruce, N. G.; Bonjour, S. *The Energy Access Situation in Developing Countries*; United Nations Development Programme (UNDP): New York, 2009; pp 1–142.

(3) Bruce, N. G.; Perez-Padilla, R.; Albalak, R. Indoor Air Pollution in Developing Countries: a Major Environmental and Public Health Challenge. *Bulletin of the World Health Organization* **2000**, *78* (9), 1078–1092.

(4) Malla, S.; Timilsina, G. R. *Household Cooking Fuel Choice and Adoption of Improved Cookstoves in Developing Countries*; The World Bank, 2014; pp 1–52.

(5) Edwards, R.; Karnani, S.; Fisher, E. M.; Johnson, M.; Naeher, L.; Smith, K. R.; Morawska, L. *WHO Indoor Air Quality Guidelines: Household Fuel Combustion*; World Health Organization, 2014; pp 1–42.

(6) Smith, K. R.; Dutta, K.; Chengappa, C.; Gusain, P. P.; Masera, O.; Berrueta, V.; Edwards, R.; Bailis, R.; Shields, K. N. Monitoring and Evaluation of Improved Biomass Cookstove Programs for Indoor Air Quality and Stove Performance: Conclusions From the Household Energy and Health Project. *Energy for Sustainable Development* **2007**, *11* (2), 5–18.

(7) Chen, C.; Zeger, S.; Breysse, P.; Katz, J.; Checkley, W.; Curriero, F. C.; Tielsch, J. M.

Estimating Indoor PM2.5 and CO Concentrations in Households in Southern Nepal: the Nepal Cookstove Intervention Trials. *PLoS ONE* **2016**, *11* (7), e0157984–17.

(8) Stanaway, J. D.; Afshin, A.; Gakidou, E.; Lim, S. S.; Abate, D.; Abate, K. H.; Abbafati, C.; Abbasi, N.; Abbastabar, H.; Abd-Allah, F.; Abdela, J.; Abdelalim, A.; Abdollahpour, I.; Abdulkader, R. S.; Abebe, M.; Abebe, Z.; Abera, S. F.; Abil, O. Z.; Abraha, H. N.; Abrham, A. R.; Abu-Raddad, L. J.; Abu-Rmeileh, N. M.; Accrombessi, M. M. K.; Acharya, D.; Acharya, P.; Adamu, A. A.; Adane, A. A.; Adebayo, O. M.; Adedoyin, R. A.; Adekanmbi, V.; Ademi, Z.; Adetokunboh, O. O.; Adib, M. G.; Admasie, A.; Adsuar, J. C.; Afanvi, K. A.; Afarideh, M.; Agarwal, G.; Aggarwal, A.; Aghayan, S. A.; Agrawal, A.; Agrawal, S.; Ahmadi, A.; Ahmadi, M.; Ahmadieh, H.; Ahmed, M. B.; Aichour, A. N.; Aichour, I.; Aichour, M. T. E.; Akbari, M. E.; Akinyemiju, T.; Akseer, N.; Al-Aly, Z.; Al-Eyadhy, A.; Al-Mekhlafi, H. M.; Alahdab, F.; Alam, K.; Alam, S.; Alam, T.; Alashi, A.; Alavian, S. M.; Alene, K. A.; Ali, K.; Ali, S. M.; Alijanzadeh, M.; Alizadeh-Navaei, R.; Aljunid, S. M.; Alkerwi, A.; Alla, F. O.; Alsharif, U.; Altirkawi, K.; Alvis-Guzman, N.; Amare, A. T.; Ammar, W.; Anber, N. H.; Anderson, J. A.; Andrei, C. L.; Androudi, S.; Animut, M. D.; Anjomshoa, M.; Ansha, M. G.; AntÃ³, J. M.; Antonio, C. A. T.; Anwari, P.; Appiah, L. T.; Appiah, S. C. Y.; Arabloo, J.; Aremu, O.; v, J. Ã. R.; Artaman, Al; Aryal, K. K.; Asayesh, H.; Ataro, Z.; Ausloos, M.; Avokpaho, E. F. G. A.; Awasthi, A.; Quintanilla, B. P. A.; Ayer, R.; Ayuk, T. B.; Azzopardi, P. S.; Babazadeh, A.; Badali, H.; Badawi, A.; Balakrishnan, K.; Bali, A. G.; Ball, K.; Ballew, S. H.; Banach, M.; Banoub, J. A. M.; Barac, A.; Barker-Collo, S. L.; rnighausen, T. W. B.; Barrero, L. H.; Basu, S.; Baune, B. T.; Bazargan-Hejazi, S.; Bedi,

N.; Beghi, E.; Behzadifar, M.; Behzadifar, M.; jot, Y. B.; Bekele, B. B.; Bekru, E. T.; Belay, E.; Belay, Y. A.; Bell, M. L.; Bello, A. K.; Bennett, D. A.; Bensenor, I. M.; Bergeron, G.; Berhane, A.; Bernabe, E.; Bernstein, R. S.; Beuran, M.; Beyranvand, T.; Bhala, N.; Bhalla, A.; Bhattarai, S.; Bhutta, Z. A.; Biadgo, B.; Bijani, A.; Bikbov, B.; Ver Bilano; Bililign, N.; Bin Sayeed, M. S.; Bisanzio, D.; Biswas, T.; rge, T. B.; Blacker, B. F.; Bleyer, A.; Borschmann, R.; Bou-Orm, I. R.; Boufous, S.; Bourne, R.; Brady, O. J.; Brauer, M.; Brazinova, A.; Breitborde, N. J. K.; Brenner, H.; Briko, A. N.; Britton, G.; Brugha, T.; Buchbinder, R.; Burnett, R. T.; Busse, R.; Butt, Z. A.; Cahill, L. E.; Cahuana-Hurtado, L.; Campos-Nonato, I. R.; rdenas, R. C.; Carreras, G.; Carrero, J. J.; Carvalho, F. L.; eda-Orjuela, C. A. C.; Rivas, J. C.; Castro, F.; pez, F. N. C. L.; Causey, K.; Cercy, K. M.; Cerin, E.; Chaiah, Y.; Chang, H.-Y.; Chang, J.-C.; Chang, K.-L.; Charlson, F. J.; Chattopadhyay, A.; Chattu, V. K.; Chee, M. L.; Cheng, C.-Y.; Chew, A.; Chiang, P. P.-C.; Chimed-Ochir, O.; Chin, K. L.; Chitheer, A.; Choi, J.-Y. J.; Chowdhury, R.; Christensen, H.; Christopher, D. J.; Chung, S.-C.; Cicuttini, F. M.; Cirillo, M.; Cohen, A. J.; Collado-Mateo, D.; Cooper, C.; Cooper, O. R.; Coresh, J.; Cornaby, L.; Cortesi, P. A.; Cortinovis, M.; Costa, M.; Cousin, E.; Criqui, M. H.; Cromwell, E. A.; Cundiff, D. K.; Daba, A. K.; Dachew, B. A.; Dadi, A. F.; Damasceno, A. A. M.; Dandona, L.; Dandona, R.; Darby, S. C.; Dargan, P. I.; Daryani, A.; Gupta, Das, R.; Neves, das, J.; Dasa, T. T.; Dash, A. P.; Davitoiu, D. V.; Davletov, K.; la Cruz-GÃ ngora, De, V.; La Hoz, De, F. P.; De Leo, D.; De Neve, J.-W.; Degenhardt, L.; Deiparine, S.; Dellavalle, R. P.; Demoz, G. T.; rrez, E. D.-G.; Deribe, K.; Dervenis, N.; Deshpande, A.; Jarlais, Des, D. C.; Dessie, G. A.; Deveber, G. A.; Dey, S.; Dharmaratne, S. D.; Dhimal, M.; Dinberu, M. T.; Ding, E. L.; Diro, H. D.; Djalalinia, S.;

Do, H. P.; Dokova, K.; Doku, D. T.; Doyle, K. E.; Driscoll, T. R.; Dubey, M.; Dubljanin, E.; Duken, E. E.; Duncan, B. B.; Duraes, A. R.; Ebert, N.; Ebrahimi, H.; Ebrahimpour, S.; Edvardsson, D.; Effiong, A.; Eggen, A. E.; Bcheraoui, El, C.; El-Khatib, Z.; Elyazar, I. R.; Enayati, A.; Endries, A. Y.; Er, B.; Erskine, H. E.; Eskandarieh, S.; Esteghamati, A.; Estep, K.; Fakhim, H.; Faramarzi, M.; Fareed, M.; Farid, T. A.; Farinha, C. S. E. S.; Farioli, A.; Faro, A.; Farvid, M. S.; Farzaei, M. H.; Fatima, B.; Fay, K. A.; Fazaeli, A. A.; Feigin, V. L.; Feigl, A. B.; Fereshtehnejad, S.-M.; Fernandes, E.; Fernandes, J. C.; Ferrara, G.; Ferrari, A. J.; Ferreira, M. L.; Filip, I.; Finger, J. D.; Fischer, F.; Foigt, N. A.; Foreman, K. J.; Fukumoto, T.; Fullman, N.; FÃ¼rst, T.; Furtado, J. O. M.; Futran, N. D.; Gall, S.; Gallus, S.; Gamkrelidze, A.; Ganji, M.; Garcia-Basteiro, A. L.; Gardner, W. M.; Gebre, A. K.; Gebremedhin, A. T.; Gebremichael, T. G.; Gelano, T. F.; Geleijnse, J. M.; Geramo, Y. C. D.; Gething, P. W.; Gezae, K. E.; Ghadimi, R.; Ghadiri, K.; Falavarjani, K. G.; Ghasemi-Kasman, M.; Ghimire, M.; Ghosh, R.; Ghoshal, A. G.; Giampaoli, S.; Gill, P. S.; Gill, T. K.; Gillum, R. F.; Ginawi, I. A.; Giussani, G.; Gnedovskaya, E. V.; Godwin, W. W.; Goli, S.; s, H. G. M.-D.; Gona, P. N.; Gopalani, S. V.; Goulart, A. C.; Grada, A.; Grams, M. E.; Grosso, G.; Gugnani, H. C.; Guo, Y.; Gupta, R.; Gupta, R.; Gupta, T.; rrez, R. A. G.; rrez-Torres, D. S. G.; Haagsma, J. A.; Habtewold, T. D.; Hachinski, V.; Hafezi-Nejad, N.; Hagos, T. B.; Hailegiyorgis, T. T.; Hailu, G. B.; Haj-Mirzaian, A.; Haj-Mirzaian, A.; Hamadeh, R. R.; Hamidi, S.; Handal, A. J.; Hankey, G. J.; Hao, Y.; Harb, H. L.; Harikrishnan, S.; Haro, J. M.; Hassankhani, H.; Hassen, H. Y.; Havmoeller, R.; Hawley, C. N.; Hay, S. I.; Hedayatizadeh-Omran, A.; Heibati, B.; Heidari, B.; Heidari, M.; Hendrie, D.; Henok, A.; Heredia-Pi, I.; Herteliu, C.; Heydarpour, F.; Heydarpour, S.;

626 Hibstu, D. T.; Higazi, T. B.; Hilawe, E. H.; Hoek, H. W.; Hoffman, H. J.; Hole, M. K.;
627 Rad, E. H.; Hoogar, P.; Hosgood, H. D.; Hosseini, S. M.; Hosseinzadeh, M.; Hostiuc,
628 M.; Hostiuc, S.; Hoy, D. G.; Hsairi, M.; Hsiao, T.; Hu, G.; Hu, H.; Huang, J. J.; Hussen,
629 M. A.; Huynh, C. K.; Iburg, K. M.; Ikeda, N.; Ilesanmi, O. S.; Iqbal, U.; Irvani, S. S. N.;
630 Irvine, C. M. S.; Islam, S. M. S.; Islami, F.; Jackson, M. D.; Jacobsen, K. H.; Jahangiry,
631 L.; Jahanmehr, N.; Jain, S. K.; Jakovljevic, M.; James, S. L.; Jassal, S. K.; Jayatilleke, A.
632 U.; Jeemon, P.; Jha, R. P.; Jha, V.; Ji, J. S.; Jonas, J. B.; Jonnagaddala, J.; Shushtari, Z.
633 J.; Joshi, A.; Jozwiak, J. J.; JÃ¼risson, M.; Kabir, Z.; Kahsay, A.; Kalani, R.; Kanchan,
634 T.; Kant, S.; Kar, C.; Karami, M.; Matin, B. K.; Karch, A.; Karema, C.; Karimi, N.;
635 Karimi, S. M.; Kasaeian, A.; Kassa, D. H.; Kassa, G. M.; Kassa, T. D.; Kassebaum, N.
636 J.; Katikireddi, S. V.; Kaul, A.; Kawakami, N.; Kazemi, Z.; Karyani, A. K.; Kefale, A.
637 T.; Keiyoro, P. N.; Kemp, G. R.; Kengne, A. P.; Keren, A.; Kesavachandran, C. N.;
638 Khader, Y. S.; Khafaei, B.; Khafaie, M. A.; Khajavi, A.; Khalid, N.; Khalil, I. A.; Khan,
639 G.; Khan, M. S.; Khan, M. A.; Khang, Y.-H.; Khater, M. M.; Khazaei, M.; Khazaie, H.;
640 Khoja, A. T.; Khosravi, A.; Khosravi, M. H.; Kiadaliri, A. A.; Kiirithio, D. N.; Kim, C.-
641 I.; Kim, D.; Kim, Y.-E.; Kim, Y. J.; Kimokoti, R. W.; Kinfu, Y.; Kisa, A.; Kissimova-
642 Skarbek, K.; ki, M. K.; Knibbs, L. D.; Knudsen, A. K. S.; Kochhar, S.; Kokubo, Y.;
643 Kolola, T.; Kopec, J. A.; Kosen, S.; Koul, P. A.; Koyanagi, A.; Kravchenko, M. A.;
644 Krishan, K.; Krohn, K. J.; Kromhout, H.; Defo, B. K.; Bicer, B. K.; Kumar, G. A.;
645 Kumar, M.; Kuzin, I.; Kyu, H. H.; Lachat, C.; Lad, D. P.; Lad, S. D.; Lafranconi, A.;
646 Lalloo, R.; Lallukka, T.; Lami, F. H.; Lang, J. J.; Van C Lansingh; Larson, S. L.; Latifi,
647 A.; Lazarus, J. V.; Lee, P. H.; Leigh, J.; Leili, M.; Leshargie, C. T.; Leung, J.; Levi, M.;
648 Lewycka, S.; Li, S.; Li, Y.; Liang, J.; Liang, X.; Liao, Y.; Liben, M. L.; Lim, L.-L.;

649 Linn, S.; Liu, S.; Lodha, R.; Logroscino, G.; Lopez, A. D.; Lorkowski, S.; Lotufo, P. A.;
650 Lozano, R.; Lucas, T. C. D.; Lunevicius, R.; Ma, S.; Macarayan, E. R. K.; Machado, Ã.
651 S. E.; Madotto, F.; Mai, H. T.; Majdan, M.; Majdzadeh, R.; Majeed, A.; Malekzadeh, R.;
652 Malta, D. C.; Mamun, A. A.; Manda, A.-L.; Manguerra, H.; Mansournia, M. A.;
653 Mantovani, L. G.; Maravilla, J. C.; Marcenes, W.; Marks, A.; Martin, R. V.; Martins, S.
654 C. O.; Martins-Melo, F. R. N.; rz, W. M.; Marzan, M. B.; Massenburg, B. B.; Mathur,
655 M. R.; Mathur, P.; Matsushita, K.; Maulik, P. K.; Mazidi, M.; McAlinden, C.; McGrath,
656 J. J.; McKee, M.; Mehrotra, R.; Mehta, K. M.; Mehta, V.; Meier, T.; Mekonnen, F. A.;
657 Melaku, Y. A.; Melese, A.; Melku, M.; Memiah, P. T. N.; Memish, Z. A.; Mendoza, W.;
658 Mengistu, D. T.; Mensah, G. A.; Mensink, G. B. M.; Mereta, S. T.; Meretoja, A.;
659 Meretoja, T. J.; Mestrovic, T.; Mezgebe, H. B.; Miazgowski, B.; Miazgowski, T.;
660 Millear, A. I.; Miller, T. R.; Miller-Petrie, M. K.; Mini, G. K.; Mirarefin, M.; Mirica, A.;
661 Mirrakhimov, E. M.; Misganaw, A. T.; Mitiku, H.; Moazen, B.; Mohajer, B.;
662 Mohammad, K. A.; Mohammadi, M.; Mohammadifard, N.; Mohammadnia-Afrouzi, M.;
663 Mohammed, S.; Mohebi, F.; Mokdad, A. H.; Molokhia, M.; Momeniha, F.; Monasta, L.;
664 Moodley, Y.; Moradi, G.; Moradi-Lakeh, M.; Moradinazar, M.; Moraga, P.; Morawska,
665 L.; Morgado-Da-Costa, J.; Morrison, S. D.; Moschos, M. M.; Mouodi, S.; Mousavi, S.
666 M.; Mozaffarian, D.; Mruts, K. B.; Muche, A. A.; Muchie, K. F.; Mueller, U. O.;
667 Muhammed, O. S.; Mukhopadhyay, S.; Muller, K.; Musa, K. I.; Mustafa, G.; Nabhan, A.
668 F.; Naghavi, M.; Naheed, A.; Nahvijou, A.; Naik, G.; Naik, N.; Najafi, F.; Nangia, V.;
669 Nansseu, J. R.; Nascimento, B. R.; Neal, B.; Neamati, N.; Negoi, I.; Negoi, R. I.;
670 Neupane, S.; Newton, C. R. J.; Ngunjiri, J. W.; Nguyen, A. Q.; Nguyen, G.; Nguyen, H.
671 T.; Nguyen, H. L. T.; Nguyen, H. T.; Nguyen, M.; Nguyen, N. B.; Nichols, E.; Nie, J.;

Ningrum, D. N. A.; Nirayo, Y. L.; Nishi, N.; Nixon, M. R.; Nojomi, M.; Nomura, S.; Norheim, O. F.; Noroozi, M.; Norrving, B.; Noubiap, J. J.; Nouri, H. R.; Shiadeh, M. N.; Nowroozi, M. R.; Nsoesie, E. O.; Nyasulu, P. S.; Obermeyer, C. M.; Odell, C. M.; Ofori-Asenso, R.; Ogbo, F. A.; Oh, I.-H.; Oladimeji, O.; Olagunju, A. T.; Olagunju, T. O.; Olivares, P. R.; Olsen, H. E.; Olusanya, B. O.; Olusanya, J. O.; Ong, K. L.; Ong, S. K.; Oren, E.; Orpana, H. M.; Ortiz, A.; Ota, E.; Otstavnov, S. S.; verland, S. Ã.; Owolabi, M. O.; A, M. P.; Pacella, R.; Pakhare, A. P.; Pakpour, A. H.; Pana, A.; Panda-Jonas, S.; Park, E.-K.; Parry, C. D. H.; Parsian, H.; Patel, S.; Pati, S.; Patil, S. T.; Patle, A.; Patton, G. C.; Paudel, D.; Paulson, K. R.; Ballesteros, W. C. P.; Pearce, N.; Pereira, A.; Pereira, D. M.; Perico, N.; Pesudovs, K.; Petzold, M.; Pham, H. Q.; Phillips, M. R.; Pillay, J. D.; Piradov, M. A.; Pirsaheb, M.; Pischon, T.; Pishgar, F.; Plana-Ripoll, O.; Plass, D.; Polinder, S.; Polkinghorne, K. R.; Postma, M. J.; Poulton, R.; Pourshams, A.; Poustchi, H.; Prabhakaran, D.; Prakash, S.; Prasad, N.; Purcell, C. A.; Purwar, M. B.; Qorbani, M.; Radfar, A.; Rafay, A.; Rafiei, A.; Rahim, F.; Rahimi, Z.; Rahimi-Movaghar, A.; Rahimi-Movaghar, V.; Rahman, M.; Rahman, M. H. U.; Rahman, M. A.; Rai, R. K.; Rajati, F.; Rajsic, S.; Raju, S. B.; Ram, U.; Ranabhat, C. L.; Ranjan, P.; Rath, G. K.; Rawaf, D. L.; Rawaf, S.; Reddy, K. S.; Rehm, C. D.; Rehm, J.; Reiner, R. C., Jr; Reitsma, M. B.; Remuzzi, G.; Renzaho, A. M. N.; Resnikoff, S.; Reynales-Shigematsu, L. M.; Rezaei, S.; Ribeiro, A. L. P.; Rivera, J. A.; Roba, K. T.; rez, S. R. G.-R.; Roever, L.; n, Y. R.; Ronfani, L.; Roshandel, G.; Rostami, A.; Roth, G. A.; Rothenbacher, D.; Roy, A.; Rubagotti, E.; Rushton, L.; Sabanayagam, C.; Sachdev, P. S.; Saddik, B.; Sadeghi, E.; Moghaddam, S. S.; Safari, H.; Safari, Y.; Safari-Faramani, R.; Safdarian, M.; Safi, S.; Safiri, S.; Sagar, R.; Sahebkar, A.; Sahraian, M. A.; Sajadi, H. S.; Salam,

N.; Salamati, P.; Saleem, Z.; Salimi, Y.; Salimzadeh, H.; Salomon, J. A.; Salvi, D. D.; Salz, I.; Samy, A. M.; Sanabria, J.; o, M. D. S.-N.; nchez-Pimienta, T. G. S.; Sanders, T.; Sang, Y.; Santomauro, D. F.; Santos, I. S.; Santos, J. O. V.; Milicevic, M. M. S.; Jose, B. P. S.; Sardana, M.; Sarker, A. R.; rez, R. S.-S.; Sarrafzadegan, N.; Sartorius, B.; Sarvi, S.; Sathian, B.; Satpathy, M.; Sawant, A. R.; Sawhney, M.; Saylan, M.; Sayyah, M.; Schaeffner, E.; Schmidt, M. I.; Schneider, I. J. C.; Ben SchÃ ttker; Schutte, A. E.; Schwebel, D. C.; Schwendicke, F.; Scott, J. G.; Seedat, S.; Sekerija, M.; Sepanlou, S. G.; Serre, M. L.; n-Mori, E. S.; Seyedmousavi, S.; Shabaninejad, H.; Shaddick, G.; Shafieesabet, A.; Shahbazi, M.; Shaheen, A. A.; Shaikh, M. A.; Levy, T. S.; Shams-Beyranvand, M.; Shamsi, M.; Sharafi, H.; Sharafi, K.; Sharif, M.; Sharif-Alhoseini, M.; Sharifi, H.; Sharma, J.; Sharma, M.; Sharma, R.; She, J.; Sheikh, A.; Shi, P.; Shibuya, K.; Shiferaw, M. S.; Shigematsu, M.; Shin, M.-J.; Shiri, R.; Shirkoohi, R.; Shiue, I.; Shokraneh, F.; Shoman, H.; Shrime, M. G.; Shupler, M. S.; Si, S.; Siabani, S.; Sibai, A. M.; Siddiqi, T. J.; Sigfusdottir, I. D.; Sigurvinsdottir, R.; Silva, D. A. S.; Silva, J. O. P.; Silveira, D. G. A.; Singh, J. A.; Singh, N. P.; Singh, V.; Sinha, D. N.; Skiadaresi, E.; Skirbekk, V.; Smith, D. L.; Smith, M.; Sobaih, B. H.; Sobhani, S.; Somayaji, R.; Soofi, M.; Sorensen, R. J. D.; Soriano, J. B.; Soyiri, I. N.; Spinelli, A.; Sposato, L. A.; Sreeramareddy, C. T.; Srinivasan, V.; Starodubov, V. I.; Steckling, N.; Stein, D. J.; Stein, M. B.; Stevanovic, G.; Stockfelt, L.; Stokes, M. A.; Sturua, L.; Subart, M. L.; Sudaryanto, A.; Sufiyan, M. B.; Sulo, G.; Sunguya, B. F.; Sur, P. J.; Sykes, B. L.; Szoeke, C. E. I.; s-Seisdedos, R. T.; Tabuchi, T.; Tadakamadla, S. K.; Takahashi, K.; Tandon, N.; Tassew, S. G.; Tavakkoli, M.; Taveira, N.; Tehrani-Banihashemi, A.; Tekalign, T. G.; Tekelemedhin, S. W.; Tekle, M. G.; Temesgen, H.; Temsah, M.-H.;

718 Temsah, O.; Terkawi, A. S.; Tessema, B.; Teweldemedhin, M.; Thankappan, K. R.;
719 Theis, A.; Thirunavukkarasu, S.; Thomas, H. J.; Thomas, M. L.; Thomas, N.; Thurston,
720 G. D.; Tilahun, B.; Tillmann, T.; To, Q. G.; Tobollik, M.; Tonelli, M.; Topor-Madry, R.;
721 Torre, A. E.; s, M. T.-G.; Touvier, M.; Tovani-Palone, M. R.; Towbin, J. A.; Tran, B. X.;
722 Tran, K. B.; Truelsen, T. C.; Truong, N. T.; Tsadik, A. G.; Car, L. T.; Tuzcu, E. M.;
723 Tymeson, H. D.; Tyrovolas, S.; Ukwaja, K. N.; Ullah, I.; Updike, R. L.; Usman, M. S.;
724 Uthman, O. A.; Vaduganathan, M.; Vaezi, A.; Valdez, P. R.; van Donkelaar, A.;
725 Varavikova, E.; Varughese, S.; Vasankari, T. J.; Venkateswaran, V.;
726 Venketasubramanian, N.; Villafaina, S.; Violante, F. S.; Vladimirov, S. K.; Vlassov, V.;
727 Vollset, S. E.; Vos, T.; Vosoughi, K.; Vu, G. T.; Vujcic, I. S.; Wagnew, F. S.; Waheed,
728 Y.; Waller, S. G.; Walson, J. L.; Wang, Y.; Wang, Y.; Wang, Y.-P.; Weiderpass, E.;
729 Weintraub, R. G.; Weldegebreal, F.; Werdecker, A.; Werkneh, A. A.; West, J. J.;
730 Westerman, R.; Whiteford, H. A.; Widecka, J.; Wijeratne, T.; Winkler, A. S.; Wiyeh, A.
731 B.; Wiysonge, C. S.; Wolfe, C. D. A.; Wong, T. Y.; Wu, S.; Xavier, D.; Xu, G.; Yadgir,
732 S.; Yadollahpour, A.; Jabbari, S. H. Y.; Yamada, T.; Yan, L. L.; Yano, Y.; Yaseri, M.;
733 Yasin, Y. J.; Yeshaneh, A.; Yimer, E. M.; Yip, P.; Yisma, E.; Yonemoto, N.; Yoon, S.-
734 J.; Yotebieng, M.; Younis, M. Z.; Yousefifard, M.; Yu, C.; Zaidi, Z.; Bin Zaman, S.;
735 Zamani, M.; Zavala-Arciniega, L.; Zhang, A. L.; Zhang, H.; Zhang, K.; Zhou, M.;
736 Zimsen, S. R. M.; Zodpey, S.; Murray, C. J. L.; Collaborators, G. 2. R. F. Global,
737 Regional, and National Comparative Risk Assessment of 84 Behavioural, Environmental
738 and Occupational, and Metabolic Risks or Clusters of Risks for 195 Countries and
739 Territories, 1990-2017: a Systematic Analysis for the Global Burden of Disease Study

2017. *The Lancet* **2018**, *392* (10159), 1923–1994.

(9) Foell, W.; Pachauri, S.; Spreng, D.; Zerriffi, H. Household Cooking Fuels and Technologies in Developing Economies. *Energy Policy* **2011**, *39* (12), 7487–7496.

(10) Jetter, J.; Zhao, Y.; Smith, K. R.; Khan, B.; Yelverton, T.; DeCarlo, P.; Hays, M. D. Pollutant Emissions and Energy Efficiency Under Controlled Conditions for Household Biomass Cookstoves and Implications for Metrics Useful in Setting International Test Standards. *Environ. Sci. Technol.* **2012**, *46* (19), 10827–10834.

(11) Jetter, J.; Ebersviller, S. *Test Report: BioLite HomeStove with Wood Fuel*; U.S. Environmental Protection Agency, 2015; pp 1–33.

(12) Delapena, S.; Garland, C.; Jagoe, K.; Okada, E.; Ouk, S.; Pennise, D.; Pillarisetti, A.; Steele, J. *Quantifying the Health Impacts of ACE-1 Biomass and Biogas Stoves in Cambodia*; Berkeley Air Monitoring Group, 2015; pp 1–52.

(13) Still, D.; Bentson, S.; Li, H. Results of Laboratory Testing of 15 Cookstove Designs in Accordance with the ISO/IWA Tiers of Performance. *EcoHealth* **2015**, *12*, 12–24.

(14) Sutar, K. B.; Kohli, S.; Ravi, M. R.; Ray, A. Biomass Cookstoves: a Review of Technical Aspects. *Renewable and Sustainable Energy Reviews* **2015**, *41*, 1128–1166.

(15) Lamberg, H.; Sippula, O.; Tissari, J.; Jokiniemi, J. Effects of Air Staging and Load on Fine-Particle and Gaseous Emissions From a Small-Scale Pellet Boiler. *Energy Fuels* **2011**, *25* (11), 4952–4960.

(16) Lyngfelt, A.; Leckner, B. Combustion of Wood-Chips in Circulating Fluidized Bed Boilers — NO and CO Emissions as Functions of Temperature and Air-Staging. *Fuel* **1999**, *78*, 1065–1072.

(17) Nuutinen, K.; Jokiniemi, J.; Sippula, O.; Lamberg, H.; Sutinen, J.; Horttanainen, P.; Tissari, J. Effect of Air Staging on Fine Particle, Dust and Gaseous Emissions From Masonry Heaters. *Biomass and Bioenergy* **2014**, *67*, 167–178.

(18) Okasha, F. Staged Combustion of Rice Straw in a Fluidized Bed. *Experimental Thermal and Fluid Science* **2007**, *32* (1), 52–59.

(19) Wiinikka, H.; Gebart, R. Critical Parameters for Particle Emissions in Small-Scale Fixed-Bed Combustion of Wood Pellets. *Energy Fuels* **2004**, *18* (4), 897–907.

(20) Caubel, J. J.; Rapp, V. H.; Chen, S. S.; Gadgil, A. J. Optimization of Secondary Air Injection in a Wood-Burning Cookstove: an Experimental Study. *Environ. Sci. Technol.* **2018**, *52* (7), 4449–4456.

(21) Rapp, V. H.; Caubel, J. J.; Wilson, D. L.; Gadgil, A. J. Reducing Ultrafine Particle Emissions Using Air Injection in Wood-Burning Cookstoves. *Environ. Sci. Technol.* **2016**, *50* (15), 8368–8374.

(22) Pettersson, E.; Lindmark, F.; Öhman, M.; Nordin, A.; Westerholm, R.; Boman, C. Design Changes in a Fixed-Bed Pellet Combustion Device: Effects of Temperature and Residence Time on Emission Performance. *Energy Fuels* **2010**, *24* (2), 1333–1340.

(23) Tryner, J.; Tillotson, J. W.; Baumgardner, M. E.; Mohr, J. T.; DeFoort, M. W.; Marchese, A. J. The Effects of Air Flow Rates, Secondary Air Inlet Geometry, Fuel Type, and Operating Mode on the Performance of Gasifier Cookstoves. *Environ. Sci. Technol.* **2016**, *50* (17), 9754–9763.

(24) Nussbaumer, T. Combustion and Co-Combustion of Biomass: Fundamentals, Technologies, and Primary Measures for Emission Reduction †. *Energy Fuels* **2003**, *17*

(6), 1510–1521.

(25) Vicente, E. D.; Alves, C. A. An Overview of Particulate Emissions From Residential Biomass Combustion. *Atmospheric Research* **2018**, *199*, 159–185.

(26) Soneja, S. I.; Tielsch, J. M.; Curriero, F. C.; Zaitchik, B.; Khatry, S. K.; Yan, B.; Chillrud, S. N.; Breysse, P. N. Determining Particulate Matter and Black Carbon Exfiltration Estimates for Traditional Cookstove Use in Rural Nepalese Village Households. *Environ. Sci. Technol.* **2015**, *49* (9), 5555–5562.

(27) Lienhard, J. H., V; Lienhard, J. H., IV. Velocity Coefficients for Free Jets FromSharp-Edged Orifices. *Journal of Fluids Engineering* **1984**, *106* (13), 13–17.

(28) Cushman-Roisin, B. Turbulent Jets. In *Environmental Fluid Mechanics*; New York, 2014; pp 1–9.

(29) *The Water Boiling Test*, 4 ed.; Global Alliance for Clean Cookstoves, 2014; pp 1–89.

(30) Bilsback, K. R.; Eilenberg, S. R.; Good, N.; Heck, L.; Johnson, M.; Kodros, J. K.; Lipsky, E. M.; L'Orange, C.; Pierce, J. R.; Robinson, A. L.; Subramanian, R.; Tryner, J.; Wilson, A.; Volckens, J. The Firepower Sweep Test: a Novel Approach to Cookstove Laboratory Testing. *Indoor Air* **2018**, *28* (6), 936–949.

(31) Wang, Y.; Sohn, M. D.; Wang, Y.; Lask, K. M.; Kirchstetter, T. W.; Gadgil, A. J. How Many Replicate Tests Are Needed to Test Cookstove Performance and Emissions? — Three Is Not Always Adequate. *Energy for Sustainable Development* **2014**, *20*, 21–29.

(32) Taylor, J. R. *An Introduction to Error Analysis: the Study of Uncertainties in Physical Measurements*; University Science Books: Sausalito, CA, 1997; pp 1–1.

(33) Bäfver, L. S.; Leckner, B.; Tullin, C.; Berntsen, M. Particle Emissions From Pellets

Stoves and Modern and Old-Type Wood Stoves. *Biomass and Bioenergy* **2011**, *35* (8), 3648–3655.

(34) Houshfar, E.; Skreiberg, Ø.; Løvås, T.; Todorović, D.; Sørum, L. Effect of Excess Air Ratio and Temperature on NOx Emission From Grate Combustion of Biomass in the Staged Air Combustion Scenario. *Energy Fuels* **2011**, *25* (10), 4643–4654.

(35) Kirch, T.; Birzer, C. H.; Medwell, P. R.; Holden, L. The Role of Primary and Secondary Air on Wood Combustion in Cookstoves. *International Journal of Sustainable Energy* **2018**, *37* (3), 268–277.

(36) Elmquist, M.; Cornelissen, G.; Kukulska, Z.; Gustafsson, Ö. Distinct Oxidative Stabilities of Char Versus Soot Black Carbon: Implications for Quantification and Environmental Recalcitrance. *Global Biogeochem. Cycles* **2006**, *20* (2), 1–11.

(37) Jiang, M.; Wu, Y.; Lin, G.; Xu, L.; Chen, Z.; Fu, F. Pyrolysis and Thermal-Oxidation Characterization of Organic Carbon and Black Carbon Aerosols. *Science of the Total Environment* **2011**, *409* (20), 4449–4455.

(38) Bond, T. C.; Doherty, S. J.; Fahey, D. W. Bounding the Role of Black Carbon in the Climate System: a Scientific Assessment. *J. Geophys. Res. Atmos.* **2013**, *118* (11), 5380–5552.

(39) Obaidullah, M.; Bram, S.; Verma, V. K.; De Ruyck, J. A Review on Particle Emissions From Small Scale Biomass Combustion. *International Journal of Renewable Energy Research* **2012**, *2* (1), 147–159.

(40) Garland, C.; Delapena, S.; Prasad, R.; L'Orange, C.; Alexander, D.; Johnson, M. Black Carbon Cookstove Emissions: a Field Assessment of 19 Stove/Fuel Combinations.

Atmospheric Environment **2017**, *169*, 140–149.

(41) Tissari, J.; Lyyränen, J.; Hytönen, K.; Sippula, O.; Tapper, U.; Frey, A.; Saarnio, K.; Pennanen, A. S.; Hillamo, R.; Salonen, R. O.; Hirvonen, M. R.; Jokiniemi, J. Fine Particle and Gaseous Emissions From Normal and Smouldering Wood Combustion in a Conventional Masonry Heater. *Atmospheric Environment* **2008**, *42* (34), 7862–7873.

(42) Torvela, T.; Tissari, J.; Sippula, O.; Kaivosoja, T.; Leskinen, J.; Virén, A.; Lähde, A.; Jokiniemi, J. Effect of Wood Combustion Conditions on the Morphology of Freshly Emitted Fine Particles. *Atmospheric Environment* **2014**, *87*, 65–76.

(43) Obernberger, I.; Brunner, T.; Barnthaler, G. *Fine Particulate Emissions From Modern Austrian Small-Scale Biomass Combustion Plants*, 15th European Biomass Conference & Exhibition, Berlin, Germany, May 7-11 2007.

(44) Nielsen, I. E.; Eriksson, A. C.; Lindgren, R.; Martinsson, J.; Nyström, R.; Nordin, E. Z.; Sadiktsis, I.; Boman, C.; Nøjgaard, J. K.; Pagels, J. Time-Resolved Analysis of Particle Emissions From Residential Biomass Combustion - Emissions of Refractory Black Carbon, PAHs and Organic Tracers. *Atmospheric Environment* **2017**, *165*, 179–190.

(45) Champier, D.; Bédécarrats, J. P.; Kousksou, T.; Rivaletto, M.; Strub, F.; Pignolet, P. Study of a TE (Thermoelectric) Generator Incorporated in a Multifunction Wood Stove. *Energy* **2011**, *36* (3), 1518–1526.

(46) Champier, D.; Bedecarrats, J. P.; Rivaletto, M.; Strub, F. Thermoelectric Power Generation From Biomass Cook Stoves. *Energy* **2010**, *35* (2), 935–942.

(47) Gao, H. B.; Huang, G. H.; Li, H. J.; Qu, Z. G.; Zhang, Y. J. Development of Stove-Powered Thermoelectric Generators: a Review. *Applied Thermal Engineering* **2016**, *96*,

297–310.

(48) Nuwayhid, R. Y.; Shihadeh, A.; Ghaddar, N. Development and Testing of a Domestic Woodstove Thermoelectric Generator with Natural Convection Cooling. *Energy Conversion and Management* **2005**, *46* (9-10), 1631–1643.

(49) Mal, R.; Prasad, R.; Vijay, V. K.; Verma, A. R. The Design, Development and Performance Evaluation of Thermoelectric Generator(TEG) Integrated Forced Draft Biomass Cookstove. *Procedia - Procedia Computer Science* **2015**, *52*, 723–729.

(50) Digi-Key Electronics. Fans and Thermal Management: DC Brushless Fans (BLDC). http://www.digikey.com/products/en/fans-thermal-management/dc-brushless-fans-bldc/217? (accessed September 12, 2018).

(51) Valavanidis, A.; Fiotakis, K.; Vlachogianni, T. Airborne Particulate Matter and Human Health: Toxicological Assessment and Importance of Size and Composition of Particles for Oxidative Damage and Carcinogenic Mechanisms. *Journal of Environmental Science and Health, Part C* **2008**, *26* (4), 339–362.

(52) Martins, L. D.; Martins, J. A.; Freitas, E. D.; Mazzoli, C. R.; Gonçalves, F. L. T.; Ynoue, R. Y.; Hallak, R.; Albuquerque, T. T. A.; Andrade, M. de F. Potential Health Impact of Ultrafine Particles Under Clean and Polluted Urban Atmospheric Conditions: a Model-Based Study. *Air Qual Atmos Health* **2010**, *3* (1), 29–39.

(53) Chen, R.; Bin Hu; Liu, Y.; Xu, J.; Yang, G.; Xu, D.; Chen, C. Beyond PM2.5: the Role of Ultrafine Particles on Adverse Health Effects of Air Pollution. *BBA - General Subjects* **2016**, *1860* (12), 2844–2855.

(54) Clifford, S.; Mazaheri, M.; Salimi, F.; Ezz, W. N.; Yeganeh, B.; Low-Choy, S.; Walker,

K.; Mengersen, K.; Marks, G. B.; Morawska, L. Effects of Exposure to Ambient Ultrafine Particles on Respiratory Health and Systemic Inflammation in Children. *Environment International* **2018**, *114*, 167–180.

(55) Just, B.; Rogak, S.; Kandlikar, M. Characterization of Ultrafine Particulate Matter From Traditional and Improved Biomass Cookstoves. *Environ. Sci. Technol.* **2013**, *47* (7), 3506–3512.

(56) Shen, G.; Gaddam, C. K.; Ebersviller, S. M.; Vander Wal, R. L.; Williams, C.; Faircloth, J. W.; Jetter, J. J.; Hays, M. D. A Laboratory Comparison of Emission Factors, Number Size Distributions, and Morphology of Ultrafine Particles From 11 Different Household Cookstove-Fuel Systems. *Environ. Sci. Technol.* **2017**, *51* (11), 6522–6532.

(57) Kelz, J.; Brunner, T.; Obernberger, I.; Jalava, P.; Hirvonen, M. R. *PM Emissions From Old and Modern Biomass Combustion Systems and Their Health Effects,* Proceedings of the 18th European Biomass Conference, Lyon, France, May 2010; ETA - Florence Renewable Energies: Florence, Italy, 2010.

(58) Johansson, L. S.; Leckner, B.; Gustavsson, L.; Cooper, D.; Tullin, C.; Potter, A. Emission Characteristics of Modern and Old-Type Residential Boilers Fired with Wood Logs and Wood Pellets. *Atmospheric Environment* **2004**, *38* (25), 4183–4195.

(59) Wiinikka, H.; Gebart, R. The Influence of Air Distribution Rate on Particle Emissions in Fixed Bed Combustion of Biomass. *Combustion Science and Technology* **2005**, *177* (9), 1747–1766.

(60) Hosseini, S.; Li, Q.; Cocker, D.; Weise, D.; Miller, A.; Shrivastava, M.; Miller, J. W.; Mahalingam, S.; Princevac, M.; Jung, H. Particle Size Distributions From Laboratory-

Scale Biomass Fires Using Fast Response Instruments. *Atmos. Chem. Phys.* **2010**, *10* (16), 8065–8076.

(61) Fox, R. W.; McDonald; Pritchard, P. J. *Introduction to Fluid Mechanics*, 7 ed.; John Wiley & Sons: Hoboken, 2017.

(62) Hay, N.; Spencer, A. Discharge Coefficients of Cooling Holes with Radiused and Chamfered Inlets. *Journal of Turbomachinery* **1992**, *114* (701), 1–6.

(63) Taslim, M.; Ugarte, S. Discharge Coefficient Measurements for Flow Through Compound-Angle Conical Holes with Cross-Flow. *The International Journal of Rotating Machinery* **2004**, *10* (2), 145–153.

(64) Incropera, F.; Dewitt, D.; Bergman, T.; Levine, A. *Fundamentals of Heat and Mass Transfer*, 6 ed.; John Wiley & Sons : Hoboken, 2007; pp 1–10.

(65) Frigge, M.; Hoaglin, D. C.; Iglewicz, B. Some Implementations of the Boxplot. *The American Statistician* **1989**, *43* (1), 50–54.

(66) Hand, J. L.; Kreidenweis, S. M. A New Method for Retrieving Particle Refractive Index and Effective Density From Aerosol Size Distribution Data. *Aerosol Science and Technology* **2002**, *36* (10), 1012–1026.

(67) Pitz, M.; Schmid, O.; Heinrich, J.; Birmili, W.; Maguhn, J.; Zimmermann, R.; Wichmann, H.-E.; Peters, A.; Cyrys, J. Seasonal and Diurnal Variation of $PM_{2.5}$ Apparent Particle Density in Urban Air in Augsburg, Germany. *Environ. Sci. Technol.* **2008**, *42* (14), 5087–5093.

(68) Khlystov, A.; Stanier, C.; Pandis, S. N. An Algorithm for Combining Electrical Mobility and Aerodynamic Size Distributions Data When Measuring Ambient Aerosol. *Aerosol*

916 *Science and Technology* **2004**, *38* (S1), 229–238.

917

Appendix A. Materials and Methods

A.1 Modular Air Injection Cookstove Design: Version 2 (MOD2)

The MOD2 stove is a wood-burning cookstove that enables the experimental optimization of secondary air injection design parameters. Figure A1 and Figure A2 below provide a rear and top view of the MOD2 stove, respectively, showing the location of the secondary air supply line, thermocouples, and manifold pressure port. Figure A2 also shows the junctures at the top of the manifold that leaked during testing. The outer juncture was sealed with a high-temperature graphite gasket (Figure A3(b)), but the thin top plate warped over extended use and thermal cycling (Figure A3(a)), resulting in leakage. Figure A1 shows that secondary air is injected into the manifold through a removable access port, which can be easily modified to accommodate a small electric fan or blower in future studies.

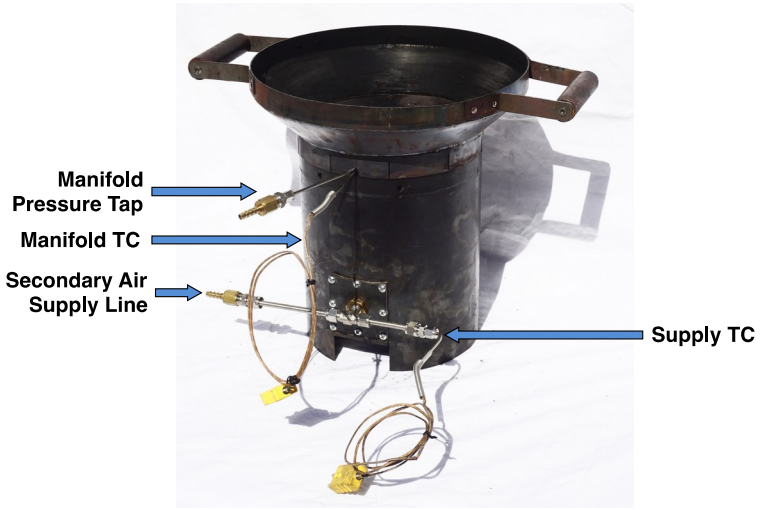

Figure A1. Rear view of the MOD2 stove, showing the secondary air inlet, thermocouples (TC), and manifold pressure port.

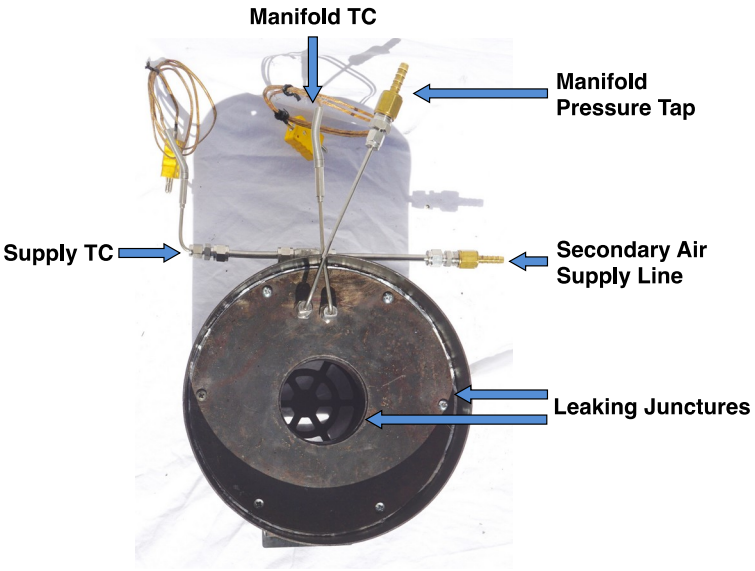

Figure A2. Top view of the MOD2 stove, showing the secondary air inlet, thermocouples (TC), manifold pressure port, and the leaky manifold junctures. The pot skirt and pot supports were removed so as to expose the top of the manifold assembly.

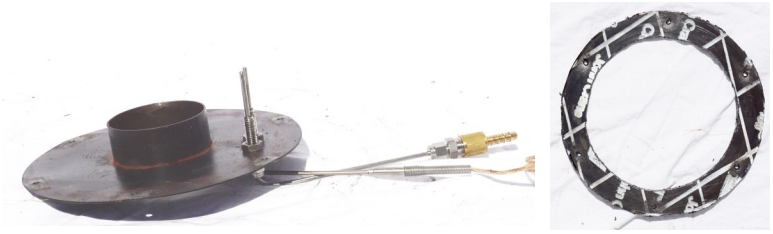

Figure A3. (a) Top of the manifold assembly, showing the thermocouple and pressure port that extend into the manifold. (b) High temperature graphite gasket, used to seal the outer juncture between the top of the manifold assembly and the stove body.

A.2 Preliminary Testing Procedure

Over the course of 52 preliminary tests, a total of 7 injection patterns were evaluated at secondary flow rates ranging from 14 to 43 SLPM (the total flow into the stove manifold). For all

patterns, the air injection orifices had a diameter of 1.59 mm (0.0625 in). Primary air flow was controlled using adjustable intakes located under the grate. During the first 8 tests, a constant firepower setting of 4 to 5 kW was difficult to maintain and the combustion efficiency was low, thereby indicating that the stove lacked primary air. Consequently, the adjustable air intakes below the grate were fully opened, and when this did not prove sufficient, the stove was also elevated on three bricks, such that primary air could flow more freely through the grate and into the bottom of the firebox. The stove was operated in this configuration for the remaining 44 trials of the preliminary testing phase.

In order to modulate the height of the pot above the chimney throat, 2.5-mm (0.10-inch) thick washers were added under the three bolts that serve as pot supports. For 17 of the first 18 tests, the stove was operated with two washers stacked under the pot support. However, as the air injection flow rate and pattern were modulated to reduce emissions, thermal efficiency tended to suffer. As a result, the supports were reduced to a single washer for all remaining trials, in an effort to maximize heat transfer to the pot. The stove was not fitted with a pot skirt or thermocouples during preliminary testing, and so no secondary air temperature data were collected.

A.3 Parametric Testing Procedure

Using the data collected during the preliminary testing phase, two promising air injection patterns were identified for further parametric testing (as outlined in Appendix B.1). Pattern 1 consisted of two concentric rows, each with three orifices evenly spaced around the circumference of the conical chimney. The bottom row of orifices were located ~6.4 mm (0.25 inch) above the juncture of the conical chimney and firebox, while the top row was located ~25

965 mm (1.0 inch) below the throat. The orifices in each row were offset, such that orifices in the top
966 row were exactly above the midpoint between two orifices in the bottom row. Pattern 2 was
967 identical to Pattern 1, except that the bottom row had six evenly spaced orifices, rather than
968 three. The two rows in Pattern 2 were vertically aligned, such that orifices in the top row were
969 directly above every other orifice in the bottom row. Both patterns are shown in Figure A4.

970 During the first 13 parametric tests, the height of the pot above the chimney throat was
971 incrementally increased from ~1.59 to 2.5 cm (~ 0.625 to 1.0 inch) to reduce the impingement of
972 flames on the bottom of the pot, but was not increased past this set point so as to enhance thermal
973 performance (larger gaps between the pot and skirt diminish convective heat transfer from the
974 exhaust gases). For the remaining 47 trials, the pot height was held constant at 2.5 cm (1.0 inch)
975 using three washers stacked under each of the bolt supports. Throughout the parametric testing
976 phase, the primary air intake was set to the fully open position. Due to fears that the stove may
977 have tipped over when elevated on three refractory bricks, 11 of the 59 parametric tests were
978 conducted with the stove placed on a piece of sheet metal. However, the stove did not seem more
979 stable in this configuration, and so all other tests were conducted using the three bricks for the
980 sake of consistency.

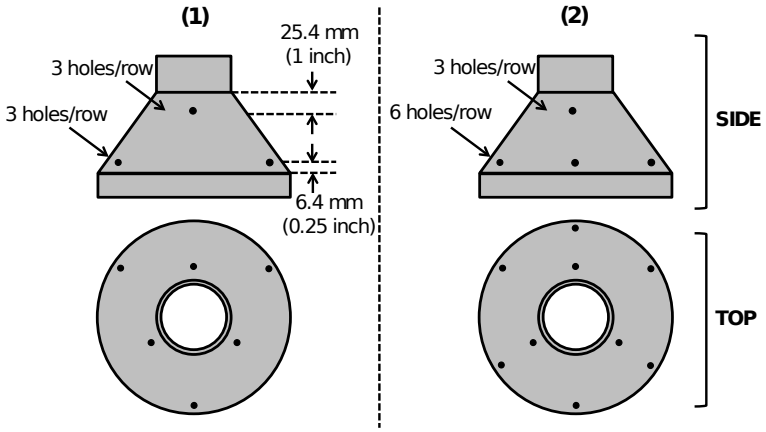

981

Figure A4. Schematic representation of the two injection patterns (Pattern 1 and Pattern 2) identified during preliminary testing, and evaluated through parametric testing. All air injection orifices have a diameter of 1.59 mm (0.0625 inch). Schematic is not drawn to scale.

A.4 Manifold Leakage Correction

The MOD2 stove's integrated manifold had some faulty juncture seals (Figure A2), and so a portion of the secondary air systematically leaked to the environment, rather than flowing through the orifices in the injection pattern and into the combustion chamber (firebox). While the stove was cold, the manifold was completely sealed using hot glue (Figure A5) to calculate the portion of the secondary flow injected through the orifices. For the two air injection patterns identified during preliminary testing, Figure A6 shows the manifold pressure at secondary flow rates ranging from 14 to 57 SLPM, with the manifold both in the normal operating configuration (leaking) and fully sealed using hot glue. Manifold pressure measurements were collected with the stove at ambient conditions throughout. Figure A6 shows that for both air injection patterns, the manifold pressure was much greater once the junctures were sealed with hot glue.

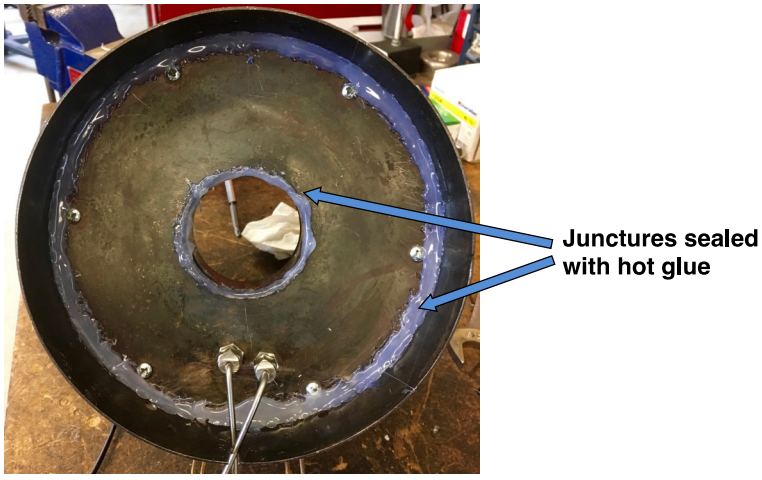

Figure A5. Top of the manifold assembly, sealed with hot glue.

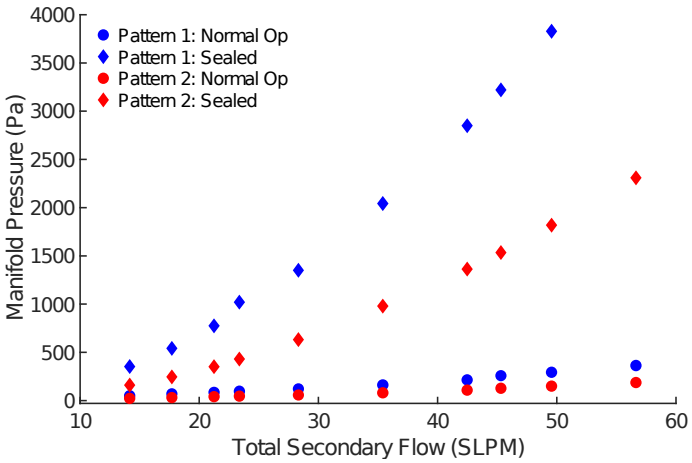

Figure A6. Manifold pressure as a function of secondary air flow rate for two injection patterns, with the manifold in both the normal operating configuration (leaking) and fully sealed using hot glue.

With the stove manifold completely sealed and all the secondary air passing through the injection pattern, it was possible to use the corresponding pressure and flow rate measurements to calculate the coefficient of discharge (C_d) through the orifices using Equation A1,

$$C_d = \left(\frac{4Q}{N\pi D^2} \right) \sqrt{\frac{\rho_{STP}}{2\Delta P}} \quad (A1)$$

where Q is the standard volumetric flow rate of secondary air (SLPM), ρ_{STP} is the density of air at standard conditions (1.225 kg/m^3), ΔP is the gauge pressure in the manifold (Pa), N is the number of orifices in the injection pattern, and D is the orifice diameter (1.59 mm).[61] The standard volumetric flow rate of secondary air into the manifold was measured with a rotameter (SLPM), and so must correspondingly be converted to mass flow rate using the density of air at standard conditions. Figure A7 below shows the coefficient of discharge calculated at each parametric setting (with the manifold fully sealed). The coefficient of discharge remains relatively constant throughout, ranging from 0.82 to 0.88, and has an average value of 0.846 ±

0.008 (mean of C_d at all parametric configurations ± 90% confidence interval). This value of discharge coefficient agrees closely with that derived in other experimental studies of turbulent air discharge through small orifices. [62,63]

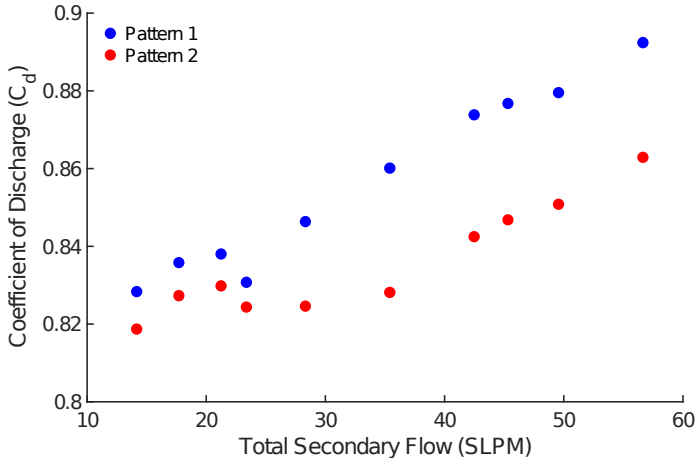

Figure A7. Coefficient of discharge (C_d) calculated at each parametric configuration, using pressure and flow rate measurements collected with the MOD2 stove manifold fully sealed, such that all the secondary air passes through orifices in each of the two injection patterns presented.

Using the average coefficient of discharge calculated above (0.846 ± 0.008) and the manifold pressure measurements collected in the normal operating configuration (with the leakage), it was possible to determine the standard volumetric flow rate of secondary air passing through each injection pattern as follows,

$$Q=\left(\frac{C_d N\pi D^2}{4}\right)\sqrt{\frac{2\Delta P}{\rho_{air}}}. \quad (A2)$$

For each combination of secondary flow rate (the total flow into the manifold) and injection pattern, Figure A8 and Figure A9 show the standard volumetric flow rate (SLPM) and fraction (%) of secondary air injected into the firebox, respectively. The flow rate of injected air increased linearly with total secondary flow, and was generally consistent between the two patterns at each

setting. As total secondary flow increased, the fraction of injected air initially decreased from 39% to 27%, presumably because higher manifold pressures pushed against the top of the manifold assembly and expanded the cracks through which air is leaking. However, the leakage stabilized for flow rates > 40 SLPM, as the cracks could expand no further.

Using these calculations, it was possible to present the stove performance results in terms of the standard volumetric flow injected through the patterns, rather than the total secondary flow into the manifold. Since secondary air leaked mostly through the outer juncture at the top of the manifold assembly, away from the firebox, it was unlikely that the leakage significantly impacted the stove's combustion performance. However, it should be acknowledged that the leakage of cold secondary air near the pot of water (the thermal load) may have hampered heat transfer from the hot exhaust flow, and potentially restricted the stove's thermal performance. Future iterations of the MOD stove should rectify the leakages, and manifold pressure measurements should be collected in real time throughout testing (as was done for temperature).

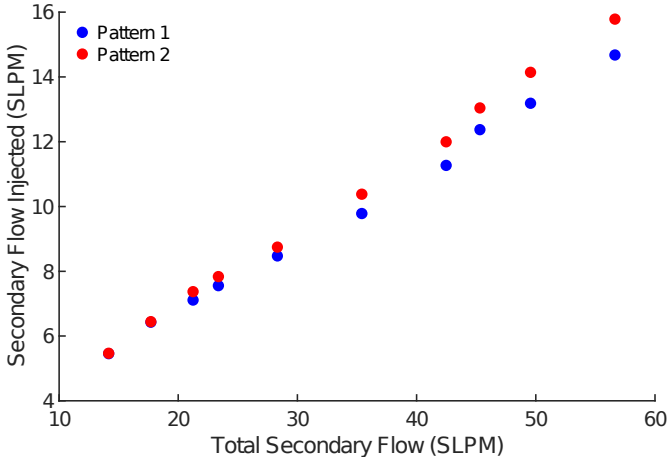

Figure A8. Standard volumetric flow rate of air injected through the orifices in each injection pattern, calculated using Equation A2, as a function of total secondary flow rate into the manifold.

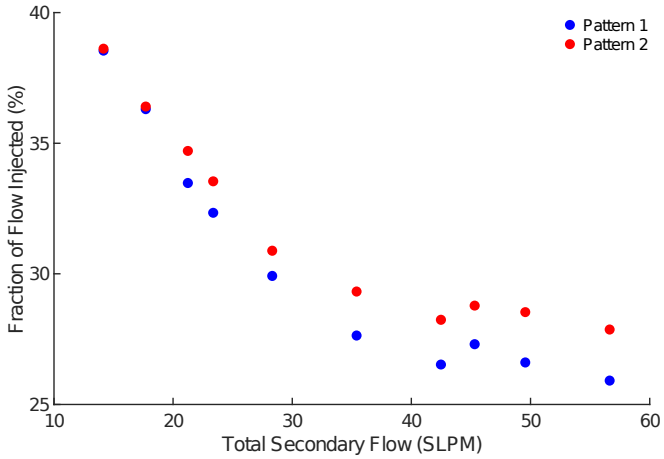

Figure A9. Fraction of the total secondary flow rate injected through the orifices in each air injection pattern.

A.5 Data Analysis and Performance Metrics

Performance metrics, such as firepower, equivalent dry mass of fuel consumed, and thermal efficiency are calculated for each test using the methods provided in the WBT Protocol 4.2.3.[29]

Emission factors are calculated according to the methods outlined by Caubel et al.,[20] and some additional methods are presented below. The total mass of gaseous emissions emitted (CO, CO_2) or consumed (O_2) is calculated using Equation A3 below,

$$m_{gas} = \sum_{t=0}^{t=t_f} \frac{10^6 \times MW \left(C_{gas}(t) - C_{gas,bkg} \right) Q_{duct}(t) P_{amb} \Delta t}{R \left(T_{duct}(t) + 273 \right)} \quad (A3)$$

where m_{gas} (g) is the total mass of gaseous emissions, t is the time step, t_f is the duration of the cold start test (sec), C_{gas} is the volumetric gas concentration (ppmv), $C_{gas,bkg}$ is the background gas concentration (ppmv), MW is the molecular weight of the gas species (g/mol), Q_{duct} is the duct flow rate (m^3/sec), P_{amb} is the ambient pressure (97150 Pa at the laboratory's altitude of ~300 m MSL), Δt is the sampling period (1 sec), R is the ideal gas constant (8.314 J/ (mol K)),

and T_{duct} is the temperature in the duct (°C). The background levels of each gas species are calculated by taking the average of concentration measurements collected for 1 min prior to the start of the test phase (ignition of the kindling), while the system is sampling ambient air. Background concentrations of $PM_{2.5}$ and BC are always assumed to be exactly 0 μg/m^3.

The average standard volumetric flow rate of air stoichiometrically consumed by the combustion (Q_{stoich}, SLPM) is calculated using Equation A4 below,

$$Q_{stoich} = \frac{4.76\, m_{O_2}\left(MW_{air}/MW_{O_2}\right)}{\rho_{STP}\, ttb} \quad (A4)$$

where m_{O2} is the total mass of O_2 consumed over the cold start (g, calculated using Equation A3), MW_{air} is the molecular of air (28.97 g/mol), MW_{O2} is the molecular mass of O_2 (32.0 g/mol), and ttb is the time to boil (min). Throughout the cold start test, the air injection velocity (v, m/s) is calculated at every time step (t) using Equation A5,

$$v(t) = \frac{4\,\rho_{STP}\, Q}{\rho(t)\,\pi N D^2} = \frac{4\,\rho_{STP}\, Q\left(T_{man}(t)+273\right) R_{air}}{P_{man}\,\pi N D^2} \quad (A5)$$

where ρ is the density of air in the manifold (kg/m^3), T_{man} is the air temperature in the manifold (°C), R_{air} is the ideal gas constant for air (287 J/Kg K), and P_{man} is the absolute pressure in the manifold (roughly equal to the local ambient pressure, 97150 Pa). Similarly, the manifold gauge pressure (ΔP, Pa) is calculated using Equation 1. The average secondary air velocity and manifold pressure are evaluated using one-second values calculated over the length of the cold start air. The average rate of heat transferred to the secondary air in the manifold (H_{man}, kW) is calculated using,

$$H_{man} = \rho_{STP}\, Q\left(C_p\left(T_{man,avg} - T_{¿,avg}\right) + \frac{1}{2}\left(4\,\rho_{STP}\, Q\, R_{air}\right)^2\left(\left(\frac{\left(T_{man,avg}+273\right)}{P_{amb}\left(N\pi D^2\right)}\right)^2 - \left(\frac{\left(T_{¿,avg}+273\right)}{P_{man}\left(\pi D_{¿}^2\right)}\right)^2\right)\right) \quad (A6)$$

where C_p is the specific heat of air (1.055 KJ/Kg K), D_{in} is the secondary air inlet diameter (4.6 mm), and $T_{man,avg}$ and $T_{in,avg}$ are the average secondary air temperatures in the manifold and inlet (°C), respectively, over the length of the test.[64]

Multiple tests were conducted for each parametric stove design configuration (unique combination of secondary air injection pattern and flow rate), and the first and third quartiles (*Q1* and *Q3*) were calculated for each replicate set of results. Outliers in each replicate set are defined as,

$$Q1 - 1.5\,IQR > outlier > Q3 + 1.5\,IQR \quad (A7)$$

where *IQR* is the interquartile range (= *Q3* – *Q1*).[65] Outliers are removed from the replicate set according to this criterion, and for each stove design configuration, the mean and 90% confidence interval of the remaining measurements (or calculated metrics) is evaluated.

Using size-resolved particle emission measurements from the TSI 3321 APS and TSI 3091 FMPS, particle density was iteratively calculated to be 1.90 ± 0.05 g/cm^3 (mean of particle density calculated for all 59 parametric stove tests ± 90% confidence interval) according to the methods presented by Caubel et al.[20] This density value agrees closely with that calculated by other researchers.[66,67] APS measurements are converted from aerodynamic to electrical mobility diameter using the calculated particle density,[68] and combined with FMPS measurements. FMPS measurements span from 6 to 340 nm, while APS measurements span from 393 to 2500 nm. The last three bins of the FMPS measurement span (from 393 to 524 nm) were discarded.

Appendix B: Supplemental Results and Discussion

B.1 Preliminary Testing Results

Testing results from all preliminary trials are provided on the first sheet of the data file entitled 'MOD2_test_results.xlsx'. The data file provides the performance and emissions metrics calculated for each individual test, and catalogs all parametric stove design configurations evaluated. In the data file, metrics highlighted in red represent outlier values not used in the calculation of configuration-average metrics (at most, only one outlier was ever removed from each set of replicate metric values). For this test phase, a total of 4 individual data points were removed from the replicate sets of measurements or output metrics. Manifold pressure measurements were only collected with air injection patterns 1 and 2, and so some operational metrics are unavailable for the remaining patterns (e.g. the calculated portion of secondary flow rate of air injected through the orifices into the firebox).

Figure B1 summarizes the thermal and emissions performance of each air injection pattern evaluated during the preliminary testing phase. For each air injection pattern, average metrics are provided for the secondary flow rate setting with the most replicate trials, shown in Figure B1(c) (please note that this represents the total secondary flow into the manifold, not the calculated portion of the flow actually injected through the orifices). Injection patterns were not systematically evaluated for a static set of secondary flow rates to reduce the total number of preliminary trials. For example, patterns were initially evaluated at secondary flow rates ranging from 18.9 to 23.5 SLPM, but it became evident that more secondary flow was required to achieve meaningful emissions reductions, and so later trials range from 28.3 to 42.5 SLPM. Although this approach reduces the comparability of the results, it allows the parametric space to be constrained rapidly prior to more methodical testing.

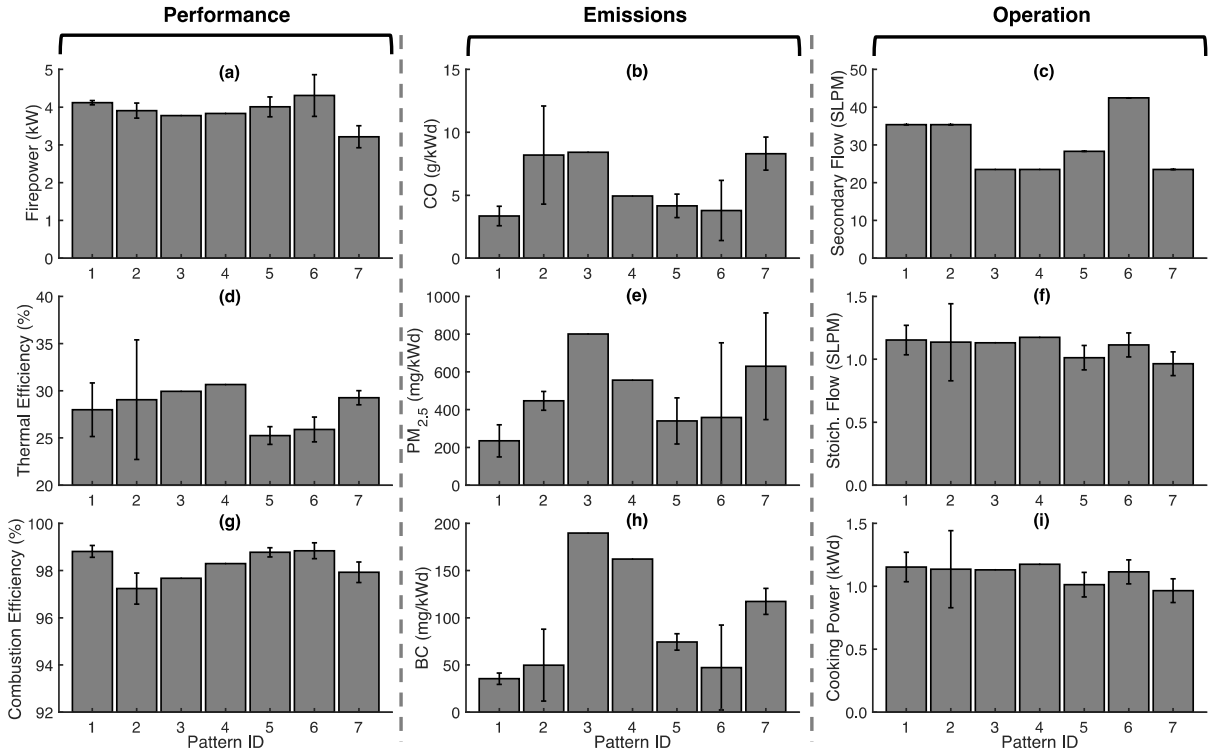

Figure B1. MOD2 stove performance, emissions, and operational metrics during high-power cold start testing (preliminary tests), presented for each air injection pattern at single secondary flow rate setting: (a) Firepower (kW); (b) CO emissions (g/KWd); (c) Total secondary flow rate into the manifold (SLPM); (d) Thermal Efficiency (%); (e) $PM_{2.5}$ emissions (mg/KWd); (f) Stoichiometric flow rate of air into the combustion (SLPM); (g) Combustion Efficiency (%); (h) BC emissions (mg/KWd); (i) Cooking Power (KWd). Bars represent the mean of replicate test data collected for each stove configuration, while error bars represent the corresponding 90% confidence interval. Only 1 test was conducted for some configurations (Patterns 3 and 4), and so confidence intervals are not shown.

Patterns 3 and 4 only had injection orifices in the bottom row (closest to the fuel bed). Visible mixing of the flame was minimal and the air jets seemed to impinge directly onto the fuel

bed. As a result, these patterns had very high BC emissions (Figure B1(h)) and were abandoned after a single experimental trial. Similarly, Pattern 7 was not considered for further testing because of elevated emissions. Pattern 7 has twelve air injection orifices, and so further testing at higher flow rates was not pursued as we sought to achieve higher air injection velocities and promote more turbulent mixing (with this aim in mind, all other injection patterns have $\leq$ 9 air injection orifices). Patterns 5 and 6 approach order-of-magnitude emissions reductions relative to the TSF, but thermal efficiency is low (~25%). Further emissions reductions would require higher secondary flow rates, which in turn would likely reduce the thermal efficiency to unacceptable levels (the thermal efficiency of the TSF is ~23%). As a result, Patterns 5 and 6 were not considered for further evaluation.

Pattern 1 was chosen for the parametric testing phase, as it had the lowest CO, $PM_{2.5}$, and BC mass emissions and maintained high thermal efficiency (~28%). Pattern 2 is nearly identical to Pattern 1, with only three additional orifices in the bottom row of the injection pattern. Although Pattern 2 has higher emissions than Pattern 1, it also achieves higher thermal efficiencies (~29%). Pattern 2 was chosen for the parametric testing phase so that the results could be compared to those from Pattern 1, and to illuminate whether the placement of air injection holes leads to a trade-off between maximizing thermal efficiency and minimizing harmful pollutant emissions. The configuration-average data presented in Figure B1 is enumerated on the first sheet of the data file entitled 'MOD2_test_summary.xlsx', and the number of replicate tests conducted for each configuration is provided.

Figure B2 and Figure B3 below summarize all the preliminary testing results collected with air injection patterns 1 and 2. For Pattern 1, 5 to 8 replicate tests were conducted at four flow rate settings, ranging from 7.2 to 12 SLPM. Only 1 or 2 tests were conduced at each of five

flow rate settings using Pattern 2, and so the corresponding confidence intervals are large or non-existent. When comparing results from the preliminary and parametric testing phases, only results collected with Pattern 1 should be considered, as insufficient trials were conducted with Pattern 2. Since thermocouples were not installed during preliminary testing, some temperature dependent parameters are omitted, such as average air injection velocity. The configuration-average data presented in Figure B2 and Figure B3 is enumerated on the first sheet of the data file entitled 'MOD2_test_summary.xlsx', and the number of replicate tests conducted for each configuration is provided.

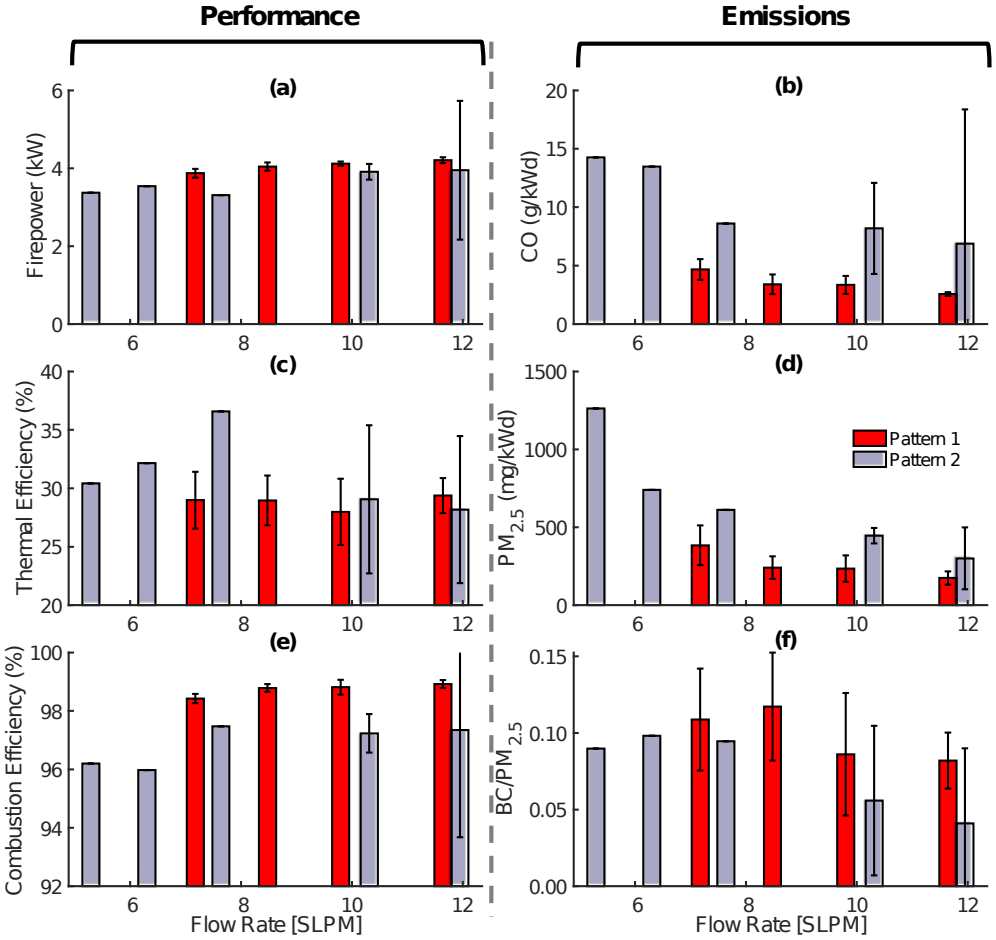

Figure B2. MOD2 stove performance, emissions, and operational metrics during high-power cold start testing (preliminary tests), presented as function of secondary air injection flow rate

and pattern: (a) Firepower (kW); (b) CO emissions (g/KWd); (c) Thermal Efficiency (%); (d) $PM_{2.5}$ emissions (mg/KWd); (e) Combustion Efficiency (%); (f) BC emissions (mg/KWd);. Bars represent the mean of replicate test data collected for each stove configuration, while error bars represent the corresponding 90% confidence interval. Only 1 test was conducted for some configurations (Pattern 2), and so confidence intervals are not shown.

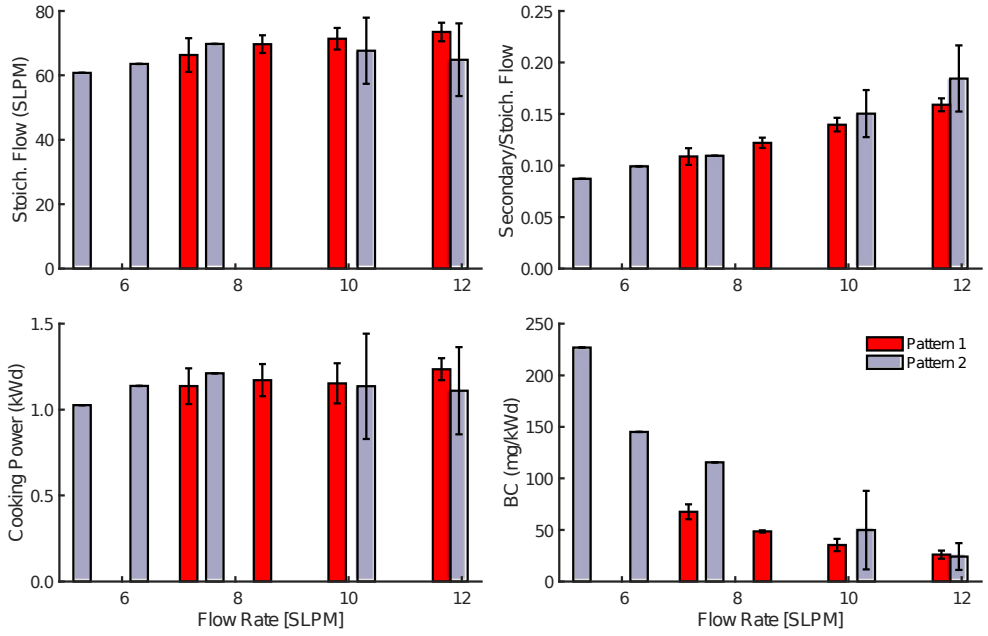

Figure B3. MOD2 stove operational metrics during high-power cold start testing (preliminary tests), presented as function of secondary air injection flow rate and pattern: (a) Stoichiometric flow rate of air into the combustion (SLPM); (b) Ratio of the secondary to stoichiometric flow rate of air; (c) Cooking Power (KWd); (d) BC emissions (mg/KWd). Bars represent the mean of replicate test data collected for each stove configuration, while error bars represent the corresponding 90% confidence interval. Only 1 test was conducted for some configurations (Pattern 2), and so confidence intervals are not shown.

B.2 Parametric Testing Results

During parametric testing, two air injection patterns were evaluated at six flow rate settings. Testing results from all parametric trials are provided on the second sheet of the data file entitled 'MOD2_test_results.xlsx'. In the data file, metrics highlighted in red represent outlier values not used in the calculation of configuration-average metrics (at most, only one outlier was ever removed from each set of replicate metric values). For this test phase, a total of 10 individual data points were removed from the replicate sets of measurements or output metrics. In addition to Figure 2 in the manuscript, Figure B4 summarizes the stove's performance at all twelve parametric design configurations. The configuration-average data presented in Figure 2 and Figure B4 are enumerated on the second sheet of the data file entitled 'MOD2_test_summary.xlsx', and the number of replicate tests conducted for each configuration is provided.

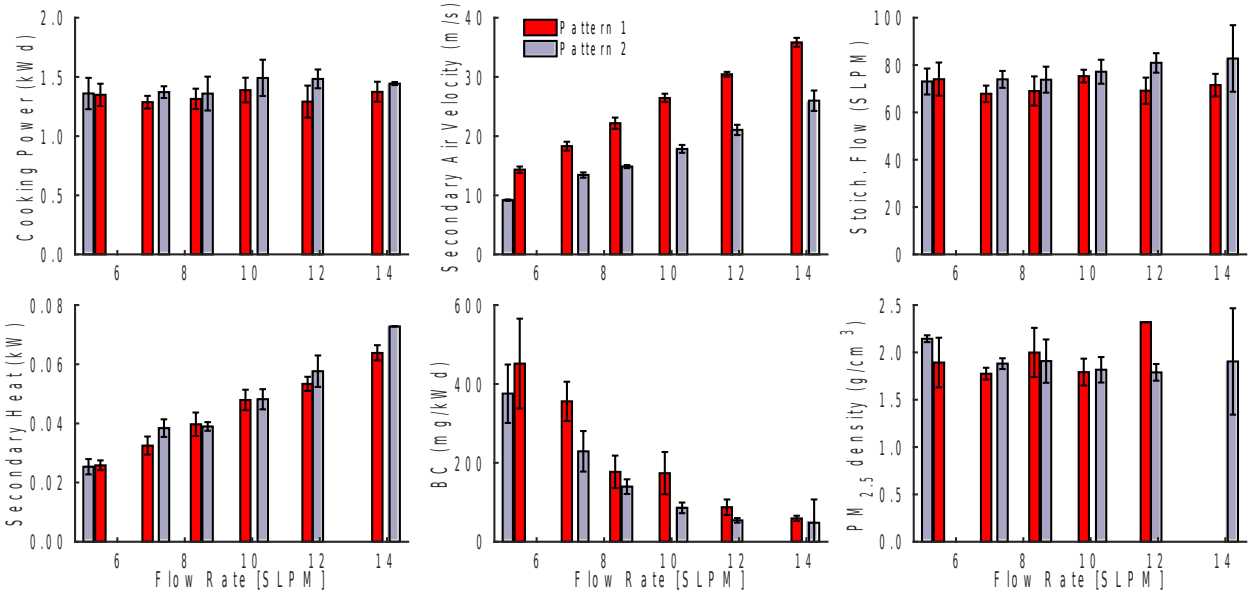

Figure B4. MOD2 stove performance, emissions, and operational metrics during high-power cold start testing, presented as function of secondary air injection flow rate and pattern: (a)

Cooking Power (kWd); (b) Average secondary air injection velocity (m/s); (c) Stoichiometric flow rate of air into the combustion (SLPM); (d) Average rate of heat transfer to secondary air in the manifold (kW); (e) Black carbon (BC) emissions (mg/kWd); (f) $PM_{2.5}$ density (g/cm^3). Bars represent the mean of replicate test data collected for each stove configuration, while error bars represent the corresponding 90% confidence interval. Error bars necessarily are omitted for metrics calculated from a single data point.

B.3 Optimal MOD2 Stove and TSF Comparison

Table B1 below summarizes the performance of the MOD2 using secondary air injection Pattern 2 at a flow rate of 12 SLPM, and compares it to a traditional three stone fire (TSF). Testing results for the TSF are provided by Rapp et al., and were collected using the same experimental set up and methods as that used during MOD2 stove testing.[21]

	TSF	MOD2	Difference (%)
Number of Tests	10	4	N/A
Firepower (kW)	5.3 (0.4)	4.7 (0.2)	-11 (8)
Time to boil (min)	31 (3)	24 (2)	-20 (10)
Cooking Power (kW)	1.22 (0.08)	1.48 (0.08)	21 (9)
Thermal Efficiency (%)	23 (1)	31 (1)	34 (6)
Combustion Efficiency (%)	95.9 (0.3)	98.95 (0.07)	3.2 (0.3)
CO (g/kWd)	18 (3)	1.7 (0.3)	-90 (20)
PM2.5 (mg/kWd)	1200 (200)	90 (20)	-90 (20)
BC (mg/kWd)	550 (40)	54 (6)	-90 (10)

Table B1. Performance and emissions metrics for a traditional three-stone fire (TSF) and the MOD2 stove in the optimal configuration (air injection Pattern 2 at 12 SLPM). The mean and 90% confidence interval (in parentheses) are provided for each metric, and the corresponding

number of replicate tests is indicated for each stove. The table also provides the percent change in MOD2 performance relative to the TSF.

B.4 $PM_{2.5}$ Generation: Additional Plots and Results

Size-resolved PM measurements were collected during parametric testing of air injection Pattern 2. For each secondary flow rate setting, Figure B5 presents the mean and 90% confidence interval of $PM_{2.5}$ emission metrics from each set of replicate cold start tests. The metrics presented in Figure B5 are identical to that shown in Figure 4 except that the emission contributions from each particle size range have been rearranged such that confidence intervals can be displayed clearly. Figure B6 presents the same $PM_{2.5}$ emission measurements as that shown in Figure 4 and Figure B5, but for three different size bins: 5 to 100 nm, 100 to 1000 nm, and 1000 to 2500 nm. This plot illustrates the emission of particles ranging from 100 to 1000 nm in diameter, which is not discernible in the other figures provided. Figure B7 and Figure B8 present the same time-resolved $PM_{2.5}$ accumulation measurements as that shown in Figure 5, but the data from the six parametric design configurations is split up over two Figures, such that 90% confidence intervals are clearly discernible. Only 2 tests were conducted at a secondary flow rate of 14 SLPM, and so the corresponding 90% confidence intervals are much larger than that shown at other secondary flow settings, for which 4 to 8 replicate tests were conducted.

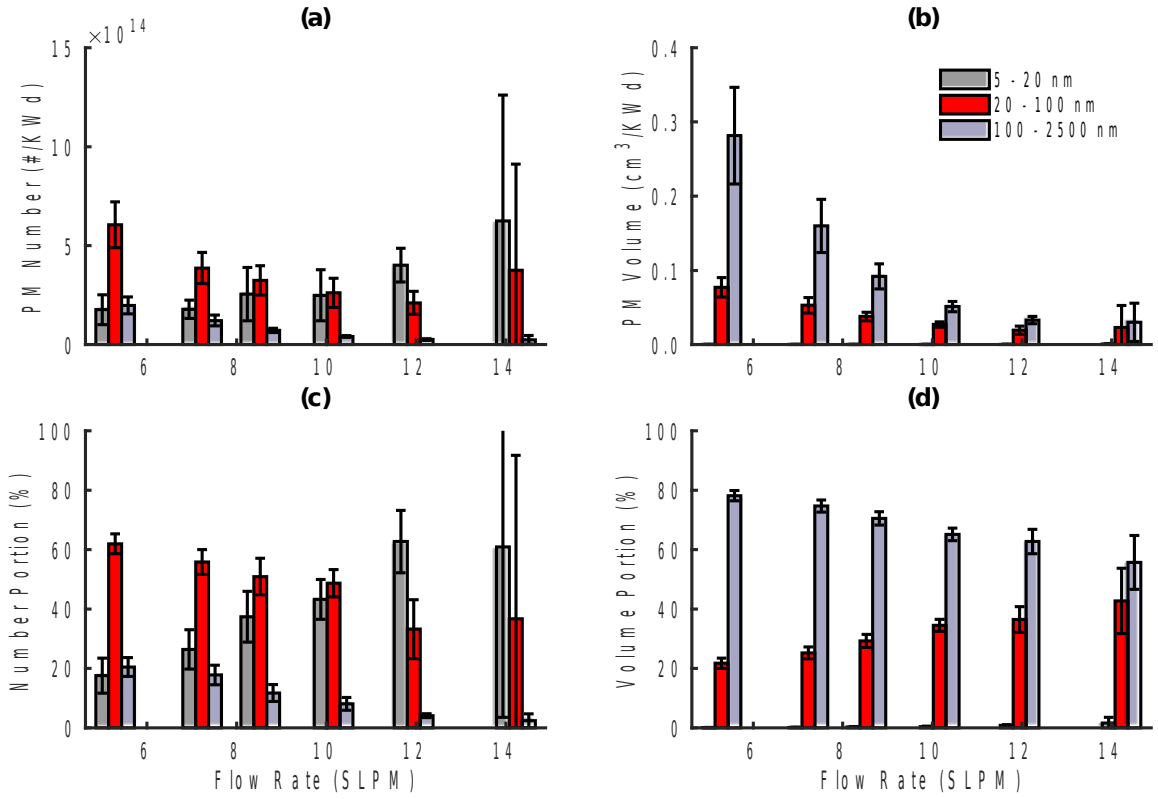

Figure B5. (a) Total $PM_{2.5}$ number and (b) volume emissions from the MOD2 stove over the cold start (normalized by cooking power), as a function of particle diameter and secondary air flow rate through injection Pattern 2. (c) Portion of the total number, and (b) volume of particles emitted in each particle diameter range: 5 to 20 nm, 20 to 100 nm, and 100 to 2500 nm. Each bar represents the mean of replicate test data collected for each stove configuration, and error bars represent the corresponding 90% confidence interval.

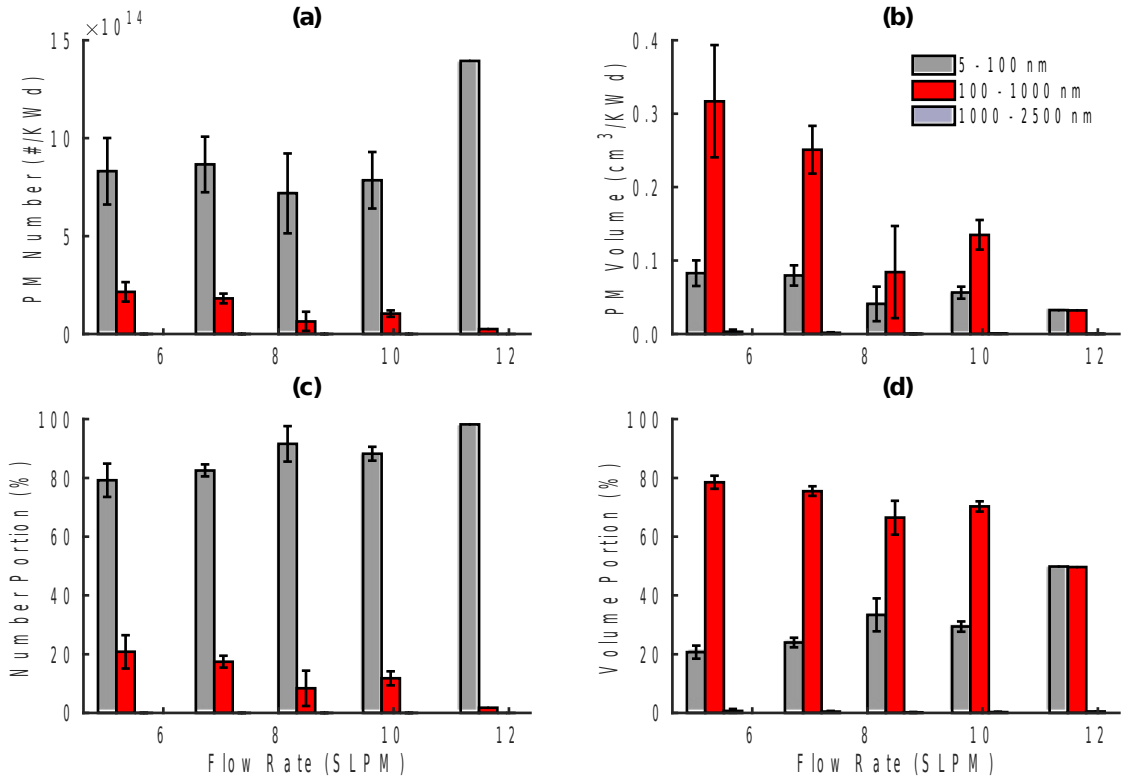

1241

1242 **Figure B6.** (a) Total $PM_{2.5}$ number and (b) volume emissions from the MOD2 stove over the
1243 cold start (normalized by cooking power), as a function of particle diameter and secondary air
1244 flow rate through injection Pattern 2. (c) Portion of the total number, and (b) volume of particles
1245 emitted in each particle diameter range: 5 to 100 nm, 1000 to 1000 nm, and 1000 to 2500 nm.
1246 Each bar represents the mean of replicate test data collected for each stove configuration, and
1247 error bars represent the corresponding 90% confidence interval.

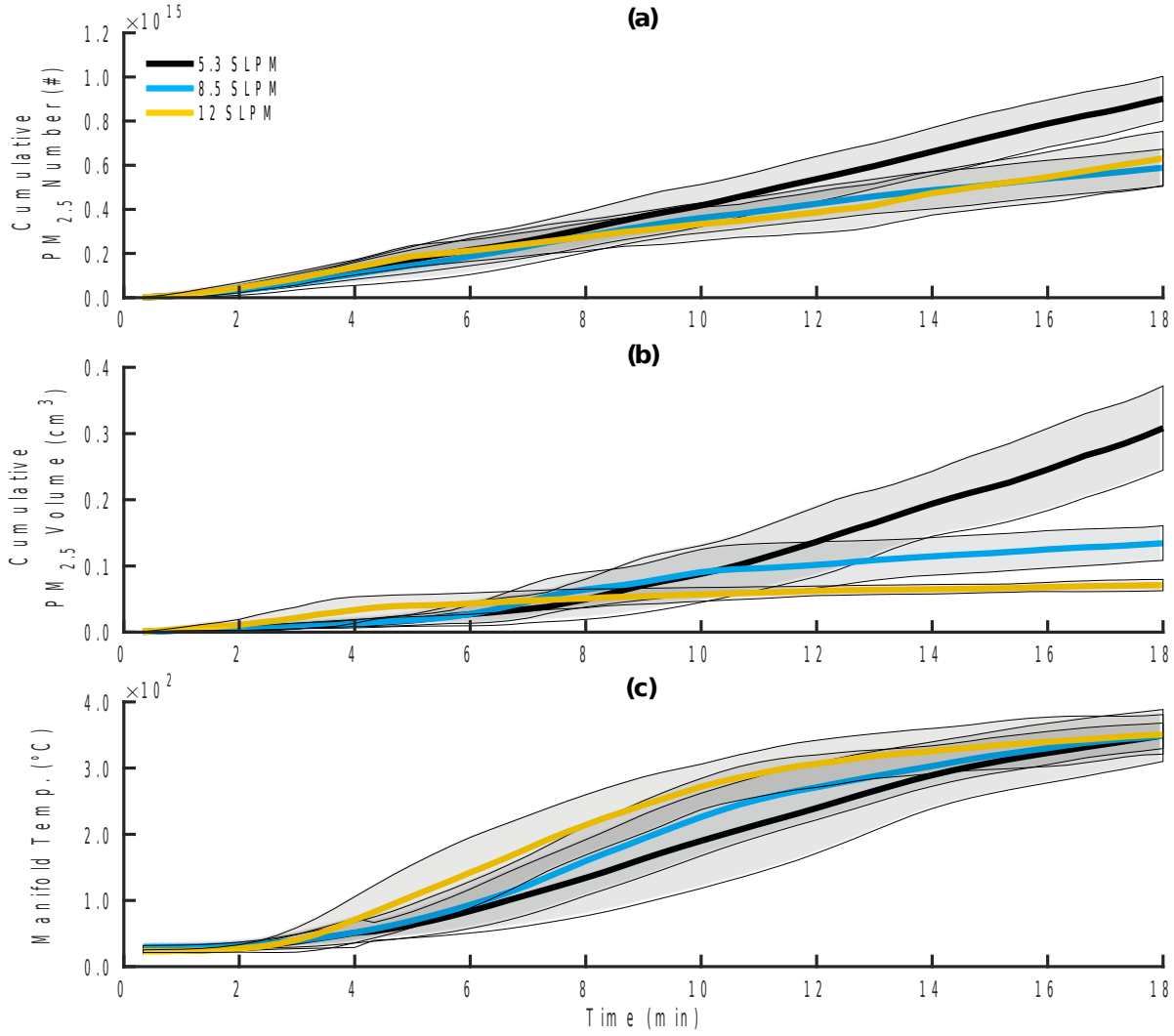

Figure B7. (a) Accumulation of $PM_{2.5}$ number and (b) volume emissions from the MOD2 stove over the first 18 minute of the cold start. (c) Temperature of secondary air in the MOD2 stove manifold over the same time period. Each bold line represents the mean of replicate test measurements collected at secondary flow settings of 5.3, 8.5, and 12 SLPM (using air injection Pattern 2), while shaded areas represent the corresponding 90% confidence interval. All data presented is block-averaged on a 20-sec time base.

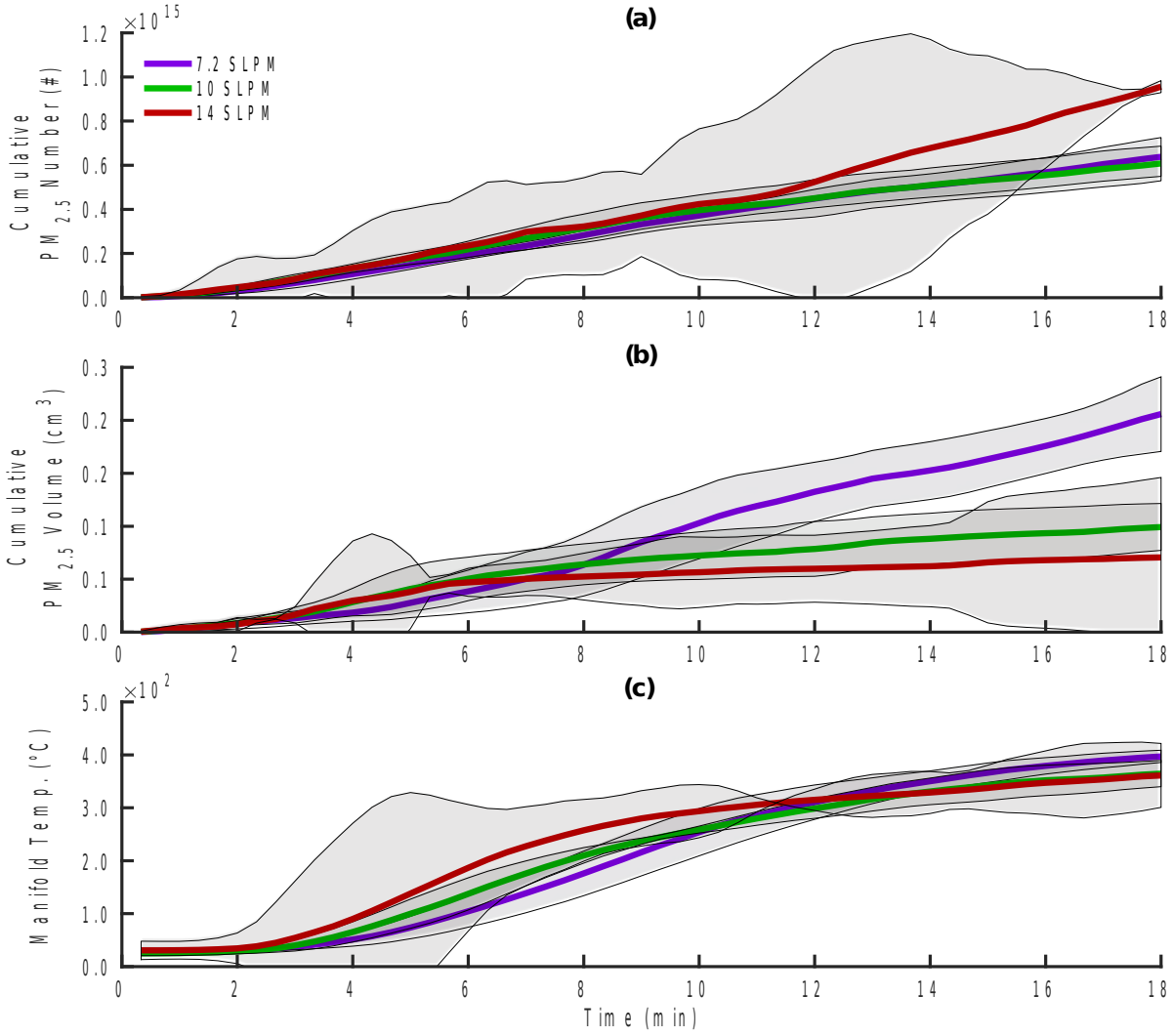

Figure B8. (a) Accumulation of $PM_{2.5}$ number and (b) volume emissions from the MOD2 stove over the first 18 minutes of the cold start. (c) Temperature of secondary air in the MOD2 stove manifold over the same time period. Each bold line represents the mean of replicate test measurements collected at secondary flow settings of 7.2, 10, and 14 SLPM (using air injection Pattern 2), while shaded areas represent the corresponding 90% confidence interval. All data presented are block-averaged on a 20-sec time base.

For each secondary flow rate setting, Figure B9 provides the size distributions of the total $PM_{2.5}$ number and volume emitted by the MOD2 stove during the cold start. Figure B10 shows the count median diameter (CMD) and volume median diameter (VMD) of $PM_{2.5}$ emissions over the first 18 minutes of the cold start. Figure B11 and Figure B12 present the same time-resolved median particle diameter data as that shown in Figure B10, but include the corresponding 90% confidence intervals at each stove configuration.

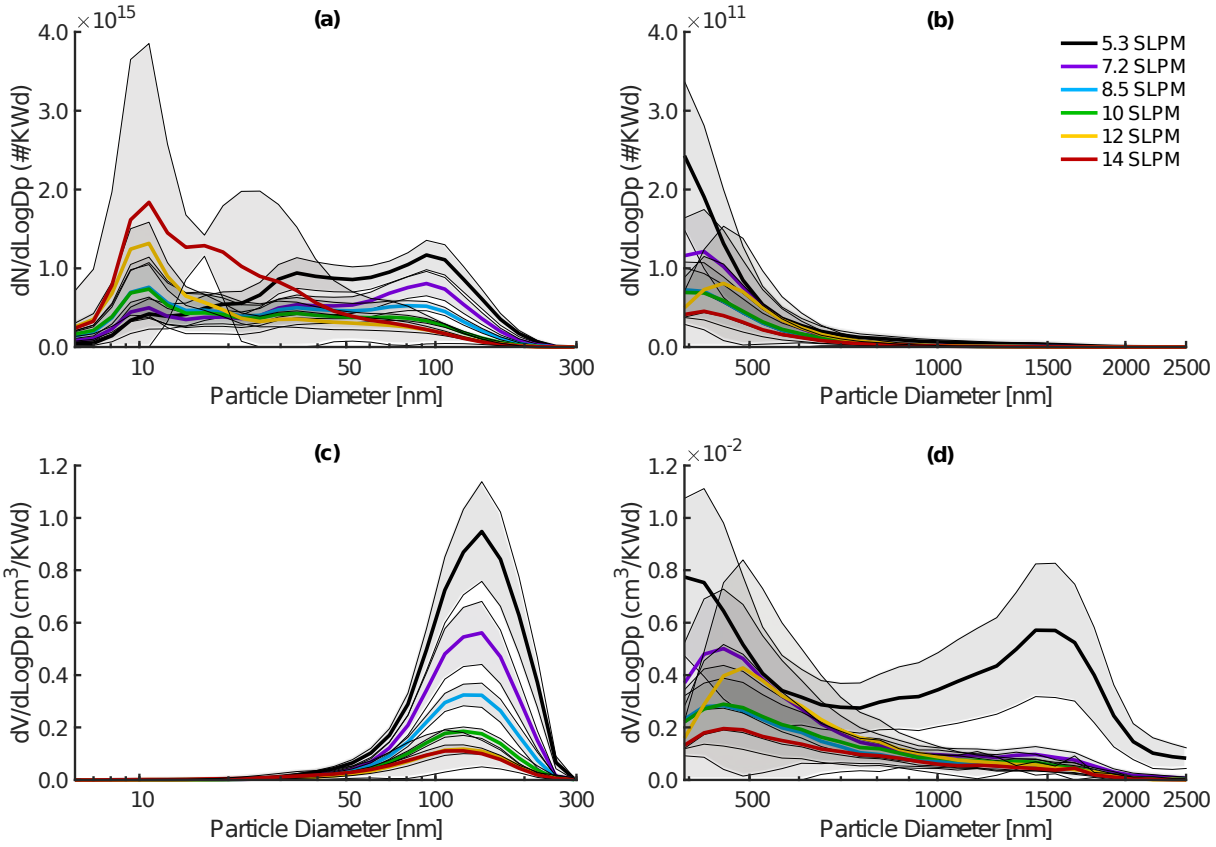

Figure B9. Size-resolved distribution of total particle number or volume emitted during the cold start, normalized by the average cooking power, for each secondary flow rate setting (using injection Pattern 2): (a) FMPS particle number distribution; (b) APS particle number distribution; (c) FMPS particle volume distribution; (d) APS particle volume distribution.

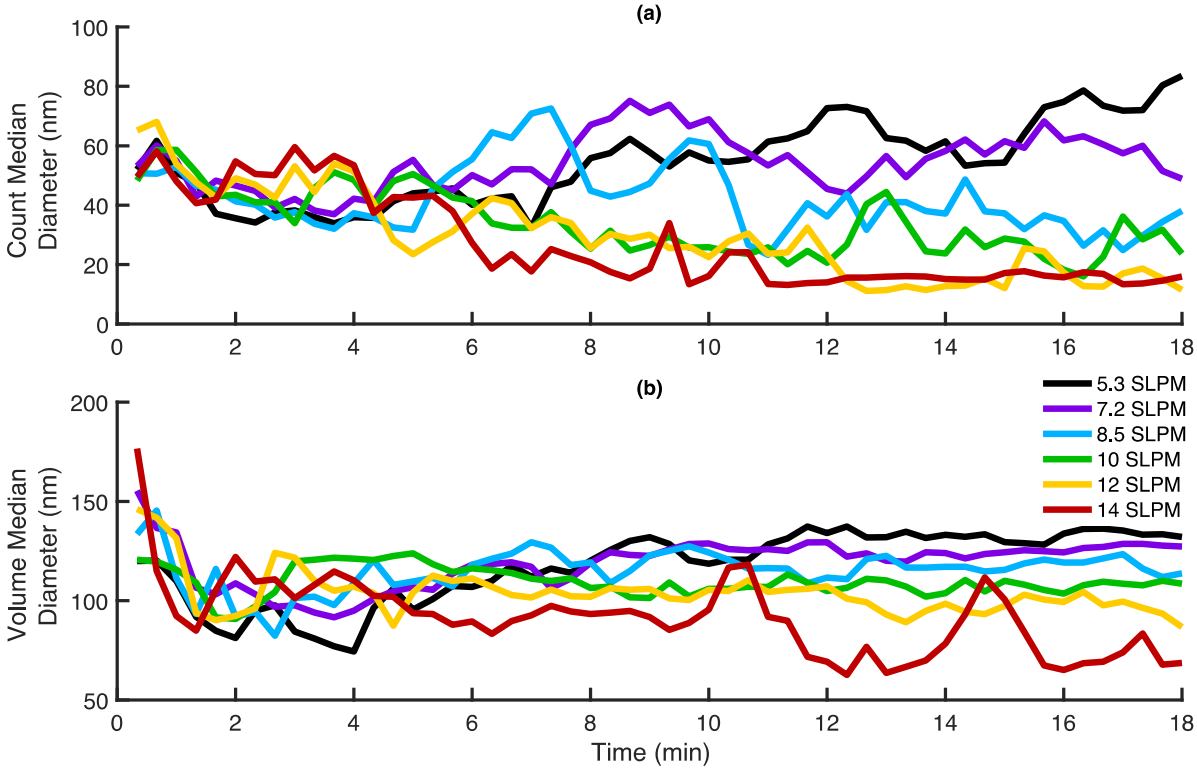

Figure B10. (a) Count median diameter and (b) count volume diameter of $PM_{2.5}$ emissions from the MOD2 stove over the first 18 minutes of the cold start. Each line represents the mean of replicate test measurements collected at each of the six secondary flow rate settings (using injection Pattern 2). Confidence are omitted here for clarity, and instead provided in Figure B11 and Figure B12 for all secondary flow rate settings. All data presented are block-averaged on a 20-sec time base.

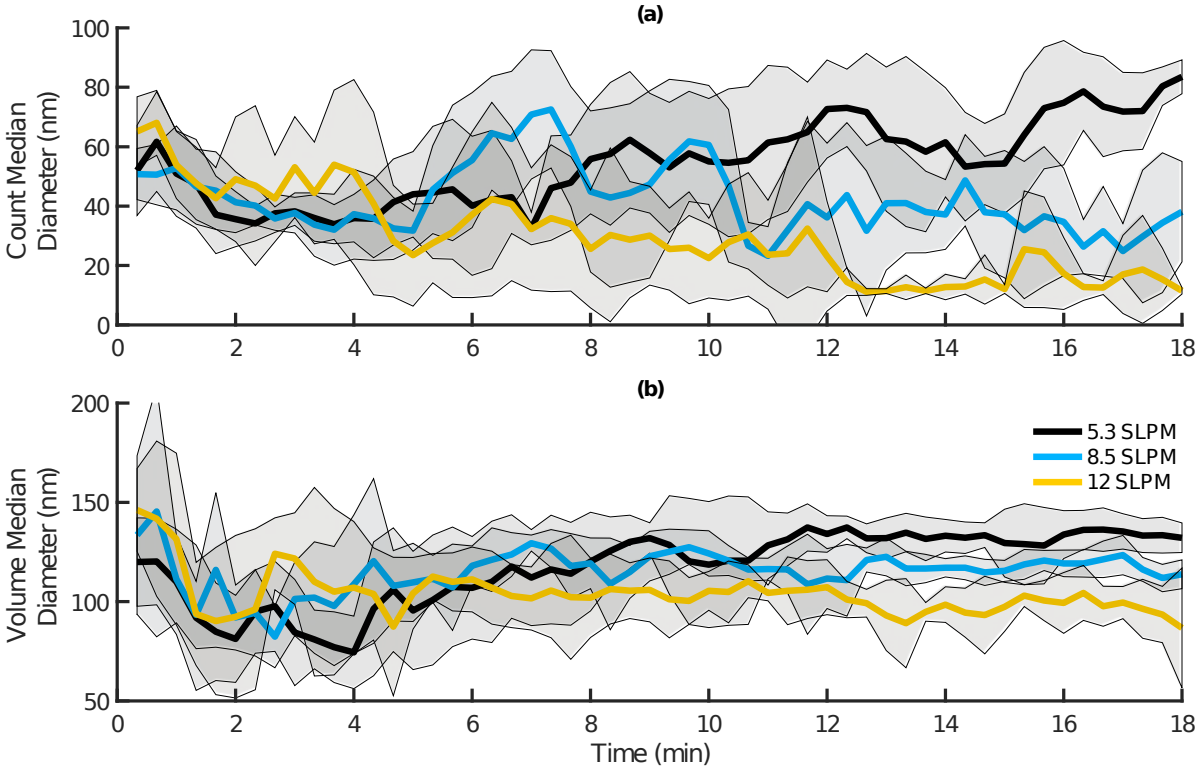

Figure B11. (a) Count median diameter and (b) count volume diameter of $PM_{2.5}$ emissions from the MOD2 stove over the first 18 minutes of the cold start. Each bold line represents the mean of replicate test measurements collected at secondary flow rate settings of 5.3, 8.5, and 12 SLPM (using air injection Pattern 2), while shaded areas represent the corresponding 90% confidence interval. All data presented are block-averaged on a 20-sec time base.

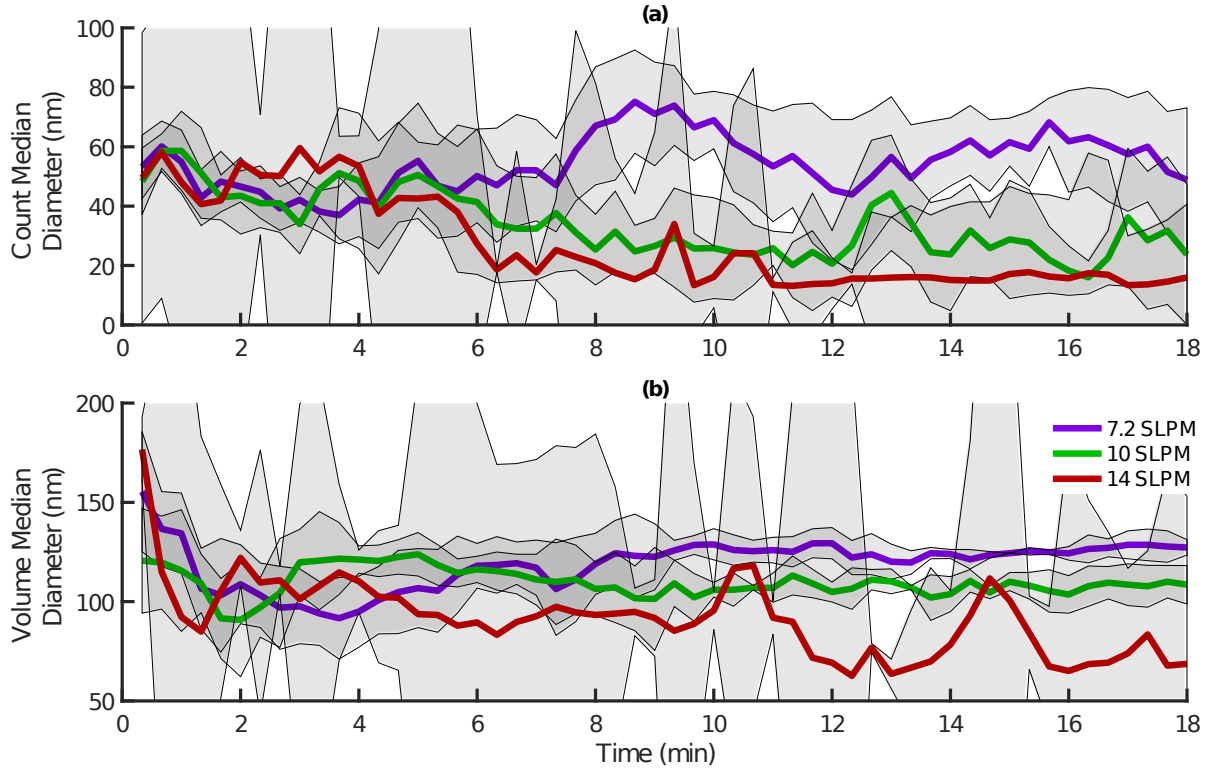

Figure B12. (a) Count median diameter and (b) count volume diameter of $PM_{2.5}$ emissions from the MOD2 stove over the first 18 minutes of the cold start. Each bold line represents the mean of replicate test measurements collected at secondary flow settings of 7.2, 10, and 14 SLPM (using air injection Pattern 2), while shaded areas represent the corresponding 90% confidence interval. All data presented are block-averaged on a 20-sec time base.

B.5 Fan and Blowers Analysis

On September 21, 2018, performance ratings and pricing information were downloaded from the Digi-Key Electronics ® website for 2,273 fans and blowers.[50] All devices costing more than $10 per unit (at an order quantity of 1000 units), rated for >10 W of electrical power consumption, or missing a classification (blower vs. fan) were removed from the set, leaving 1,135 devices remaining for analysis. The static pressure, free flow rate, and rated electrical power

consumption of these 1,135 miniature axial fans and centrifugal blowers is depicted on Figure 3. This data is also provided in the attached Excel file entitled ‘Fans_and_Blowers.xlsx’, along with the corresponding model number, pricing, and other relevant information for each device.